Analysis of the equilibrium wall model for high-speed turbulent flows

Prahladh S. Iyer*
National Institute of Aerospace, Hampton, Virginia 23666, USA

Mujeeb R. Malik†
NASA Langley Research Center, Hampton, Virginia 23681, USA

(Received 26 March 2019; published 25 July 2019)

We perform *a priori* and *a posteriori* analyses of the equilibrium wall model for high-speed wall-bounded turbulent flows. The time-averaged flow from various direct numerical simulation (DNS) databases is used as input to the wall model and the accuracy of the predictions in terms of wall shear stress and wall temperature (or heat flux for isothermal wall boundary conditions) are assessed. Two different mixing-length-based eddy-viscosity models and various damping functions are tested in this study. Both mixing-length models involve two adjustable parameters: (i) the von Kármán constant κ, which varies in the literature from 0.37 to 0.44, and (ii) a viscous damping constant A^+ (for the van Driest damping function). Also, for compressible flows, multiple scalings can be used for the viscous wall-normal spacing in the damping function. The sensitivity of the results to these model parameters is reported and it is found that the predictions of skin friction and wall temperature (or heat flux) are sensitive to the constants used, damping function scaling, and the wall-model exchange location. Wall-modeled large-eddy simulation (WMLES) is performed for (i) supersonic channel flow with a cold wall and (ii) an axisymmetric supersonic boundary layer for the adiabatic wall condition, to verify the *a priori* trends observed with respect to the damping functions. *A posteriori* WMLES results are consistent with the trends observed in the *a priori* analysis of DNS data, thus indicating the usefulness of the *a priori* analysis. We introduce a damping function scaling, which works well over a range of Mach numbers and thermal wall conditions.

DOI: 10.1103/PhysRevFluids.4.074604

I. INTRODUCTION

Many practical flows are turbulent in nature, e.g., those over cars, airplanes, and space vehicles, and predicting skin-friction drag and heat flux accurately is a crucial component of the design. The applications typically involve fluid flow at high Reynolds numbers (and Mach numbers for space vehicles) causing the flow to be turbulent. When using computational fluid dynamics in the design of such applications, various fidelities can be utilized depending on the available resources. Low-fidelity Reynolds-averaged Navier-Stokes (RANS) models involve modeling all of the turbulence and solving only for the time-averaged flow quantities. While computationally efficient, it suffers in accuracy for complex flows. Higher-fidelity scale-resolving methods such as large-eddy simulation (LES) and direct numerical simulation (DNS) are quite accurate but are computationally very expensive, especially for practical applications. Spalart *et al.* [1] estimate that a LES of an aircraft wing at flight Re (10×10^6 based on the chord) would require on the order

*prahladh.iyer@nianet.org
†mujeeb.r.malik@nasa.gov

of 100×10^9 grid points (assuming a modest 20 points per boundary-layer thickness) and 5×10^6 time steps, and thus wall-resolved LES of a full aircraft configuration would not be feasible for the foreseeable future.

The wall-modeled LES approach, in which the near-wall region is modeled with RANS while the majority of the length scales away from the wall are resolved using LES, is a reasonable compromise between accuracy and computational cost. Wall-modeled LES can further be classified into (i) stress-based wall-modeled LES (WMLES) and (ii) hybrid RANS-LES methods such as improved delayed detached eddy simulation (IDDES). In the stress-based WMLES approach, the computational grid is coarse in the wall-normal (and wall-parallel) direction, thus requiring the regular no-slip boundary condition to be supplemented by a wall shear stress (and heat flux or temperature) boundary condition (see [2–5] for overviews of stress-based WMLES). In IDDES, the grid is very fine in the wall-normal direction but coarse in the wall-parallel direction, thus requiring the LES eddy viscosity to be replaced by a RANS eddy viscosity where the majority of the turbulence is modeled (see [6–9] for an overview of the DES-based approach). In this study, we focus on the stress-based WMLES approach, which is implied when we refer to WMLES in the rest of the paper.

Stress-based WMLES can be further classified into equilibrium and nonequilibrium models depending on the level of complexity of the wall model. The equilibrium wall model neglects nonequilibrium effects such as acceleration and pressure gradient and works quite well for canonical wall-bounded flows such as channels and boundary layers. The relatively simple zero-equation mixing-length model for the eddy viscosity has been widely used in WMLES of wall-bounded turbulent flows (channel, boundary layers, and Couette flow) with reasonable success. Note that the mixing-length model involves two empirical constants for incompressible speeds, namely, the von Kármán constant κ and the damping function constant A^+ (for the van Driest function). For low-speed flows, the definition of $y^+ = yu_\tau/\nu$ in the damping function is unambiguous, whereas for high-speed flows, the wall-normal co-ordinate (y) can be nondimensionalized (to y^+) by using either the wall properties (density and viscosity) or local properties or a combination of both. While WMLES has performed well for low-speed flows [2,3], its application to high-speed flows is more recent [10–13] and has been limited in terms of the range of Mach number and thermal wall condition simulated. Note that high-fidelity DNS-LES data are scarce compared to the incompressible flow regime.

There is limited freedom to change the scalings used in the eddy-viscosity model, as the compressible law of the wall relation fixes the scaling used for the eddy viscosity in the log-layer. However, the damping function, which was first introduced by van Driest [14] for low-speed flows, is empirical with its constant A^+ set to match the correct intercept of the log-law. For compressible flows, multiple normalizations y^+ of the wall-normal coordinate y are possible, which is the main focus of this study. This has been previously investigated in the context of the k-ϵ RANS model by Aupoix and Viola [15]. They determined that the semilocal scaling yields the best results overall. In the context of WMLES with an equilibrium wall model, Kawai and Larsson [10] used the wall scaling for the damping function. Bocquet *et al.* [11] and Yang and Lv [16] compared the wall and semilocal scalings and found that the semilocal scaling works best. However, both the aforementioned studies investigated only flows with cold-wall thermal boundary conditions.

In this study, we assess the performance of the equilibrium wall model with a mixing-length-type eddy-viscosity model and different damping function scalings for the van Driest damping function, over a range of thermal boundary conditions (from adiabatic to cold wall) and Mach numbers matching available DNS databases. Note that this study does not deal with errors associated with the log-layer mismatch and uses the fix proposed by Kawai and Larsson [10] to minimize such errors in the *a posteriori* WMLES simulations. *A priori* analysis is performed with existing and new damping function scalings, and the errors in predicting the wall quantities (skin friction and temperature or heat flux) are reported at various exchange locations from which data are input to the wall model.

We empirically determine a wall-normal scaling for the van Driest damping function that appears to work best over a range of Mach numbers and thermal conditions. We also examine the sensitivity of the predictions to different mixing-length models, inclusion of pressure-gradient effects, and turbulent Prandtl number. Finally, *a posteriori* WMLESs are performed for two flow conditions, (i) Mach 3 channel flow with a cold wall and (ii) a Mach 2.85 axisymmetric turbulent boundary layer with an adiabatic wall, to test the consistency of the effect of damping function scaling from the *a priori* analysis.

This paper is organized as follows. The equilibrium-wall-model equations along with the eddy-viscosity models and damping functions are described in Sec. II. Results from the *a priori* analysis of the wall model are reported along with sensitivity to various parameters in Sec. III. The *a posteriori* WMLES results are reported for the supersonic channel and axisymmetric boundary layer in Sec. IV. The main findings are summarized in Sec. V.

II. EQUILIBRIUM WALL MODEL

The equilibrium-wall-model equations are derived from the compressible Reynolds-averaged Navier-Stokes equations with the boundary-layer approximation and neglecting nonequilibrium terms such as pressure gradient, as given by

$$\frac{d}{dy}\left[(\mu+\mu_t)\frac{du}{dy}\right]=0, \tag{1}$$

$$\frac{d}{dy}\left[(\mu+\mu_t)u\frac{du}{dy}+(k+k_t)\frac{dT}{dy}\right]=0. \tag{2}$$

Here y is the wall-normal coordinate, u is the mean wall-parallel velocity magnitude, T is the mean temperature, μ and k are the mean dynamic viscosity and thermal conductivity, respectively, and μ_t and k_t are the eddy viscosity and turbulent thermal conductivity, respectively. In the above equations, y and u are defined with reference to the corresponding wall values (i.e., $y=u=0$ at the wall). More details of the equilibrium wall model can be found in Ref. [4]. The eddy viscosity can be defined as

$$\mu_{t,\mathrm{JK}}=\rho\kappa y\sqrt{\tau_w/\rho}D, \tag{3}$$

$$\mu_{t,\mathrm{Pr}}=\rho\kappa^2y^2|du/dy|D. \tag{4}$$

The eddy viscosity for the wall model is obtained from the mixing-length model in which the length scale is taken to be κy, while the velocity scale is either taken to be the local friction velocity ($u_\tau^*=\sqrt{\tau_w/\rho}$) or the length scale multiplied by the velocity gradient ($\kappa y\frac{\partial u}{\partial y}$) as shown in Eq. (4). Here κ is the von Kármán constant, which is taken to be 0.41 in this study, but varies in literature between 0.37 and 0.44. The sensitivity of the predictions to κ is small, as discussed in Sec. III. The eddy viscosity or conductivity is multiplied by a damping function D to ensure that $\mu\gg\mu_t$ close to the wall. Note that the expression for eddy viscosity in Eq. (3) is of the same form as the Johnson-King model [17] and so, following Cabot [18], who appears to be the first to use this model, the subscript JK is used. The expression in Eq. (4) is based on the work of Prandtl [19] and so the subscript Pr is used. The eddy conductivity is computed from the eddy viscosity and specific heat of the gas (C_p), assuming a constant turbulent Prandtl number Pr_t as

$$k_t=\frac{C_p\mu_t}{\mathrm{Pr}_t}. \tag{5}$$

In the region beyond the buffer layer, typically for $y^+\gtrsim 30$ (log-law region), the turbulent stresses dominate over the viscous stresses ($\mu_t\gg\mu$), and so for large y^+, the damping function D is designed to be unity (since no damping is necessary). Under these conditions, integrating the momentum equation (1) with respect to y reduces to

$$\mu_t \frac{du}{dy} = \tau_w = \rho_w u_\tau^2. \tag{6}$$

Substituting the JK and Pr mixing-length models and setting $u_\tau = \sqrt{\tau_w/\rho_w}$, we obtain

$$\mu_{t,\mathrm{JK}} \frac{du}{dy} = \rho_w u_\tau^2 \Rightarrow \kappa y \frac{du}{dy} = \sqrt{\frac{\rho_w}{\rho}} u_\tau, \tag{7}$$

$$\mu_{t,\mathrm{Pr}} \frac{du}{dy} = \rho_w u_\tau^2 \Rightarrow (\kappa y)^2 \left|\frac{du}{dy}\right|^2 = \frac{\rho_w}{\rho} u_\tau^2. \tag{8}$$

It is straightforward to see that Eqs. (7) and (8) are identical, with the Prandtl mixing-length model giving the square of the equation obtained using the JK mixing-length model. This is the familiar compressible law of the wall relationship [20–22]. Thus, both mixing-length models seem to be appropriate as they reduce to the compressible law of the wall.

We now turn our attention to the damping function D. The most popular damping function is the one given by van Driest [14]. In this study, we also examine the damping function used in the popular Spalart-Allmaras (SA) [23] RANS model, which is in turn based on the work of Mellor and Herring [24], and a modified van Driest (VD) damping function proposed by Piomelli *et al.* [25]. Note that all the damping functions are empirical in nature with constants tuned to yield proper decay of the eddy viscosity for small y^+. The damping functions are given by

$$D_{\mathrm{VD}} = \left[1 - \exp\left(-\frac{y^+}{A^+}\right)\right]^2, \tag{9}$$

$$D_{\mathrm{SA}} = \frac{\hat{\mu}_t^3}{\hat{\mu}_t^3 + C_{v1}^3 \mu^3}, \tag{10}$$

$$D_{\mathrm{Pio}} = \left\{1 - \exp\left[-\left(\frac{y^+}{A^+}\right)^3\right]\right\}. \tag{11}$$

While the van Driest and Piomelli *et al.* [25] damping functions depend on the nondimensionalized wall-normal distance y^+, the Spalart-Allmaras damping function depends on the undamped eddy viscosity $\hat{\mu}_t$ and dynamic viscosity μ. Note that all three are empirical in nature, with corresponding empirical constants A^+ and C_{v1}. The main requirement of the damping function is that $D \approx 1$ for $y^+ \gtrsim 30$ and $D \to 0$ for $y^+ \to 0$, typically as y^2 or y^3. The constant A^+ is chosen to match the intercept in the log-law region of the velocity profile and is found to be 26 [14] for the Prandtl mixing-length model and 17 for the Johnson-King based mixing-length model when using the van Driest damping function. The sensitivity of the results to A^+ is reported in Sec. III. For constant density incompressible flows, there is no ambiguity in defining $y^+ = yu_\tau/\nu$; however, for compressible flows, multiple definitions are possible depending on whether we choose the local density or viscosity or the corresponding wall values. Note that for the SA damping function $C_{v1} = 7.1$ and the local viscosity is used for compressible flows.

A. Damping function scalings

If we define the wall friction velocity $u_\tau = \sqrt{\tau_w/\rho_w}$ and the local friction velocity as $u_\tau^* = \sqrt{\tau_w/\rho}$, multiple definitions of y^+ used in the van Driest damping function are possible, with two listed below:

$$y^+_{\mathrm{wall}} = \frac{\rho_w u_\tau y}{\mu_w},$$

$$y^+_{\mathrm{SL}} = \frac{\rho u_\tau^* y}{\mu} = \frac{\sqrt{\rho\rho_w} u_\tau y}{\mu}.$$

The wall and semilocal (SL) scalings have previously been used in the WMLES literature. For high-speed flows, the wall scaling has been used by Kawai and Larsson [10] and Bermejo-Moreno *et al.* [12], among others, while the semilocal scaling has been used by Bocquet *et al.* [11] and more recently by Yang and Lv [16]. Bocquet *et al.* [11] simulated the cold-wall Mach 3 channel flow corresponding to the DNS of Coleman *et al.* [26] (also used in this study) and found that the semilocal scaling gives improved predictions when compared to the wall scaling. Yang and Lv [16] studied the cold-wall supersonic Couette flow case and found that with the wall scalings, the error in prediction of C_f can be of the order of 100% for large Mach numbers. They however did not report the errors in the prediction of wall heat flux. The semilocal scaling and the eddy-viscosity form used in Eq. (3) can be derived from the Trettel-Larsson transformation [27] to collapse compressibility effects (see [16]). Since the Trettel-Larsson transformation was quite successful in collapsing the compressible velocity profiles to the corresponding incompressible ones (especially for cold-wall flows), one might expect that the semilocal scaling would be very accurate. However, our results suggest that this may not be the case. Also, more recently, Zhang *et al.* [28] reported that the Trettel-Larsson transformation is less successful than previously observed (e.g., [27,29]) based on their DNS of hypersonic turbulent boundary layers. In the absence of an "exact" compressible transformation, it is worth looking into other empirical scalings. In this study, we propose additional scalings as shown by

$$\begin{aligned}
y^+_{\text{local}} &= \frac{\rho u_\tau y}{\mu},\\
y^+_{\text{mixed}} &= \frac{y^+_{\text{wall}} + y^+_{\text{SL}}}{2},\\
y^+_{\text{mixed2}} &= \frac{y^+_{\text{local}} + y^+_{\text{SL}}}{2},\\
y^+_{\text{mixedmin}} &= \min(y^+_{\text{mixed}}, y^+_{\text{SL}}),\\
y^+_{\text{mixedmin2}} &= \min(y^+_{\text{mixed}}, y^+_{\text{mixed2}}).
\end{aligned}$$

The local scaling uses the local properties and u_τ instead of u^*_τ used in the semilocal scaling. The mixed scaling is a simple average of the wall and semilocal scalings, while the mixed2 scaling is the simple average of the local and semilocal scalings. The mixedmin scaling uses the minimum of the mixed and semilocal scalings, while the mixedmin2 scaling uses the minimum of the mixed and mixed2 scalings. It will be seen later that the mixed scaling works best at adiabatic conditions, while the semilocal or mixed2 scaling works best for most of the cold-wall flows considered in this study. For adiabatic flows, $T(y) < T_w$, and thus $y^+_{\text{wall}} < y^+_{\text{SL}}$, implying that $y^+_{\text{mixed}} < y^+_{\text{SL}}$. Similar reasoning for cold-wall flows implies that $y^+_{\text{mixed}} > y^+_{\text{SL}}$. Thus, the mixedmin scaling uses the minimum of the mixed and SL scalings so that it is identical to the mixed scaling for hot walls and to the semilocal scaling for cold walls. The mixedmin2 uses the same rationale but instead switches to the mixed2 scaling for cold walls. Note that all the compressible scalings obey the basic requirements of a damping function ($D \to 0$ as $y \to 0$, and $D \approx 1$ for $y^+ \gtrsim 30$) and reduce to the same $y^+ = yu_\tau/\nu$ for constant density incompressible flows. It should be noted that since the damping function itself is empirical and adjusted to yield the correct near-wall eddy-viscosity behavior, it appears that the choice of a suitable damping function scaling for high-speed flows must also be determined empirically.

B. Solution of wall-model equations

The wall-model equations listed in Eqs. (1)–(5) are solved using information from the LES solution (for a WMLES) or the DNS-LES database (for *a priori* analysis) at a certain distance from the wall and return the wall shear stress and heat flux (or wall temperature for adiabatic flows). A second-order staggered finite-difference scheme is used to solve the coupled system of equations. For the WMLES, the quantities returned by the wall model are applied as a boundary condition to the LES near-wall grid point after solving the coupled ordinary differential equations. In all the results reported, 41 grid points were used with the first grid point spacing of $\Delta y^+ < 0.1$. A further increase in grid points did not significantly alter the results. The equations were solved until a maximum residual of 10^{-8} was reached for both u/u_∞ and T/T_∞ up to a maximum of 1000 iterations. Preliminary tests were used to determine the number of grid points, number of iterations, and residual that give acceptably good grid converged results. The wall-model code was also validated with the *a priori* results of Bocquet *et al.* [11] for the cold-wall channel flows and excellent agreement was obtained. Further details about the wall model and implementation can be found in Refs. [4,10].

Historically, in WMLES, the solution from the first grid point adjacent to the wall was used as input to the wall model, but Kawai and Larsson [10] showed that the LES solution in the first few grid points is inherently erroneous. Most studies have thus chosen an exchange location of approximately 5–10% of the boundary-layer thickness δ_{99} or half-width h for channel flows, with at least three grid points between the wall the exchange location. One of the objectives of this study is to determine a suitable exchange location for a range of flow conditions.

For the *a priori* analysis, DNS data are input to the wall-model equations at different distances from the wall and the outputs of the wall model are compared to the corresponding values from DNS. The wall skin friction C_f and heat transfer parameter B_q for isothermal flows are defined as

$$C_f = \frac{\mu \frac{du}{dy}\big|_w}{\frac{1}{2}\rho_\infty u_\infty^2}, \tag{12}$$

$$B_q = \frac{-k\frac{dT}{dy}\big|_w}{\rho_w u_\tau C_p T_w}. \tag{13}$$

The error ε_Q in any wall-model output quantity Q is defined as

$$\varepsilon_Q(\%) = \left(\frac{Q_{\mathrm{wm}} - Q_{\mathrm{DNS}}}{Q_{\mathrm{DNS}}}\right) \times 100\%. \tag{14}$$

Here Q is either C_f, or B_q for isothermal walls and T_w for adiabatic walls. Note that the error ε_Q is independent of the sign convention used for any quantity Q such as B_q.

III. *A PRIORI* ANALYSIS OF DNS DATA

For the *a priori* analysis, the following publicly available turbulent DNS databases are used in this study: incompressible channel database for $\mathrm{Re}_\tau \approx 590$ flow corresponding to the study of Moser *et al.* [30] (see [31]) and $\mathrm{Re}_\tau \approx 2000$ flow corresponding to the study of Lee and Moser [32] (see [33]), incompressible boundary-layer database up to $\mathrm{Re}_\theta = 8300$ corresponding to the study of Eitel-Amor *et al.* [34] (see [35]), supersonic channel database at Mach 1.5 and Mach 3 and cold-wall conditions corresponding to the studies of Coleman *et al.* [26] (see [36]) and Modesti and Pirozzoli [29] (see [37]), supersonic turbulent boundary-layer database from Mach 2 to Mach 4 corresponding to the study of Pirozzoli and Bernardini [38–41] (see [42]) at adiabatic conditions, and supersonic-hypersonic turbulent boundary-layer database corresponding to the study of Zhang *et al.* [28] (see [43]) over a range of thermal conditions.

A. Incompressible flows

We first assess the accuracy of the wall model for incompressible flows and its sensitivity to various parameters before considering compressible flows. Since high-quality pseudospectral DNS results are available for the turbulent channel flow, we choose to assess the sensitivities for this flow. We will then check the findings for a lower-Reynolds-number channel and a turbulent boundary

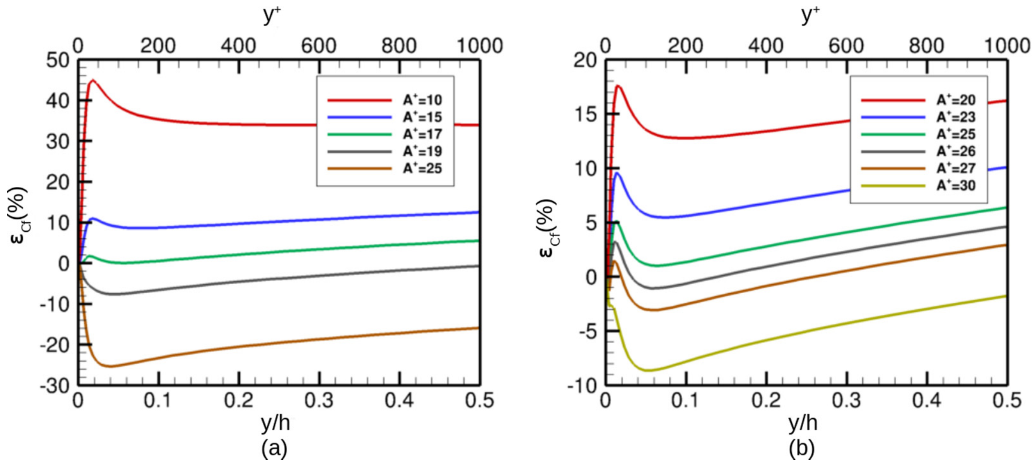

FIG. 1. Effect of the empirical constant A^+ on the wall-model predictions for the $\mathrm{Re}_\tau \approx 2000$ channel: (a) Johnson-King-type mixing-length model and (b) Prandtl mixing-length model. In this and the following plots, the abscissa is the exchange location at which data were input to the wall model.

layer. The temperature is assumed to be constant and the energy equation (2) is not solved for the results in this section.

1. The $\mathrm{Re}_\tau \approx$ **2000** *turbulent channel: Sensitivity to various parameters*

We examine the sensitivity of the wall model to the mixing-length model, damping constant A^+, and von Kármán constant κ, including dp/dx and different damping functions. We consider the $\mathrm{Re}_\tau = 1995$ channel flow corresponding to the DNS of Lee and Moser [32] for this analysis.

The sensitivity of the predictions to the empirical constant A^+ used in the van Driest damping function (9) is shown in Fig. 1 for the two mixing-length models (3) and (4). The typical value of A^+ used for the JK model by Cabot [18] and Cabot and Moin [2] is 17, while it is 26 for the Prandtl model by van Driest [14]. Although most studies use the aforementioned values of A^+ with a variation of ± 2, we intentionally choose a broader range of A^+ to understand how the errors vary with A^+. Hence, we look at the sensitivity to A^+ between 10 and 25 for the JK model and between 20 and 30 for the Prandtl model. For the results in Fig. 1 and the rest of the figures in this paper, the abscissa is the wall-normal distance from the wall at which velocity (and temperature for compressible flows) was input to the wall model (i.e., exchange location). Typically, in WMLES studies, an exchange location (y/h) between 0.05 and 0.15 is used. Therefore, in this and the following plots, this region should be the region of focus. The distance from the wall is specified in outer units (bottom axis) and viscous wall units (top axis). The error in the output quantity (C_f) defined by Eq. (14) is the ordinate of the figure. The results from Fig. 1 indicate that the wall model is highly sensitive to the value of A^+ for both the mixing-length models and the lowest error is obtained with $A^+ = 17$ for the JK model and $A^+ = 26$ for the Prandtl model, consistent with previous studies. A higher value of A^+, which implies a lower y^+/A^+ and more damping, leads to a lower value of C_f and vice versa. It is also evident that the value of A^+ is sensitive to the mixing-length model. For both models, the error in prediction (for the optimal value of A^+) is within 3% of the DNS value until $y/h \approx 0.15$. While the equilibrium-wall-model equations are technically valid only in the inner layer ($y/h < 0.15$), it can be seen that the errors are still within 5% for these two values of A^+ until $y/h \approx 0.5$. The other inference is that the performances of the two mixing-length models are equivalent in spite of the fact that the Prandtl model uses a more local velocity scale ($\kappa y du/dy$), and so we will focus more on the JK model hereafter.

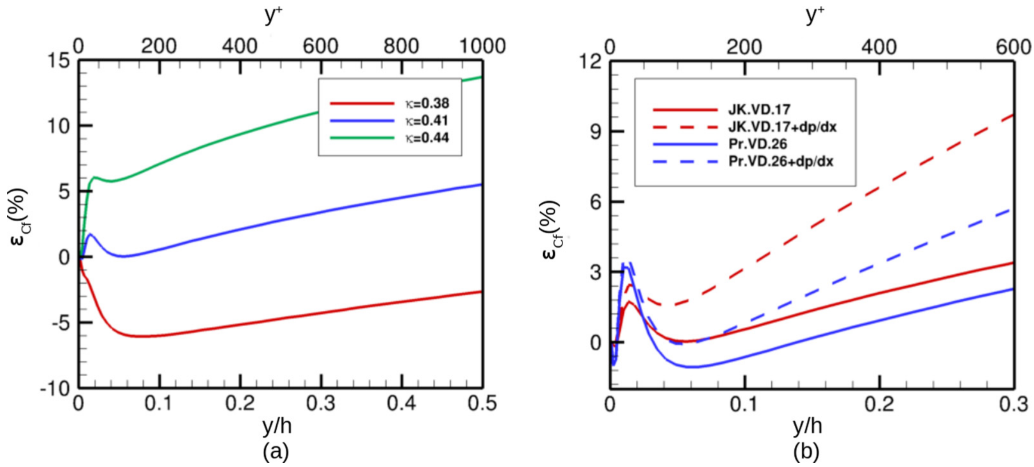

FIG. 2. Effect of (a) the von Kármán constant κ using the Johnson-King-type mixing-length model and (b) including the pressure-gradient term on the wall-model predictions with $\kappa = 0.41$ for both the Johnson-King ($A^+ = 17$) and Prandtl ($A^+ = 26$) models, for the $\mathrm{Re}_\tau \approx 2000$ channel.

The effect of the von Kármán constant κ on the predictions using the JK model and van Driest damping function (with $A^+ = 17$) is shown in Fig. 2(a) with κ varying between 0.38 and 0.44. It can be seen that there is some sensitivity (approximately 5%) to the value of κ. Overall, $\kappa = 0.41$ yields the best results in spite of the fact that the value of κ obtained from DNS data by Lee and Moser [32] and Lozano-Durán and Jiménez [44] was approximately 0.384 for channel flow at this Reynolds number. We think that this is because the value of κ and A^+ together determine the overall predictive error, and for $A^+ = 17$, a corresponding value of $\kappa = 0.41$ yields the best results. Since we are using the equilibrium model which neglects the pressure-gradient term dp/dx, it is of interest to see if including this term improves the predictions. We know for a fully developed channel flow that $dp/dx = -\tau_w/h$. We impose the dp/dx from DNS to the right-hand side of the wall-model equations (2). The Johnson-King model (with $A^+ = 17$) and the Prandtl model (with $A^+ = 26$) are considered using $\kappa = 0.41$. The results in Fig. 2(b) show that including the dp/dx term does not significantly improve the predictions, but rather makes the predictions worse for $y/h > 0.1$, possibly because the zero-equation eddy-viscosity models used do not incorporate nonequilibrium effects. For $y/h < 0.1$, we see that the effect of dp/dx is relatively small, indicating that the equilibrium assumption is reasonable very near the wall. Thus, henceforth, even though we report errors until $y/h = 0.5$, we will mainly focus on the results for $y/h \leqslant 0.1$ so that the nonequilibrium terms can be neglected in the wall model.

We compare the predictions of different mixing-length models and damping functions in Fig. 3. The JK model with VD ($A^+ = 17$) and SA damping functions and the Prandtl model with VD ($A^+ = 26$) and Piomelli *et al.* [25] damping function ($A^+ = 25$) results are shown. Overall, all the damping functions perform well for an exchange location y/h between 0.05 and 0.15 with under 3% error. However, at locations closer to the wall ($y/h \approx 0.01$), the SA and Piomelli *et al.* [25] damping functions have an error up to 8% in magnitude.

2. *The* $\mathrm{Re}_\tau \approx 590$ *channel and* $\mathrm{Re}_\tau \approx 2118$ *boundary layer*

The results for the $\mathrm{Re}_\tau \approx 2000$ channel flow have shown that the JK and Prandtl models with VD or SA (for JK) damping functions work quite well and produce an error of less than 3% when the exchange location y/h is between 0.05 and 0.15. We now check the performance for a lower-Re channel at $\mathrm{Re}_\tau \approx 590$ corresponding to the results of Moser *et al.* [30] and a zero-pressure-gradient boundary layer at $\mathrm{Re}_\tau \approx 2118$ corresponding to the results of Eitel-Amor *et al.* [34]. The same

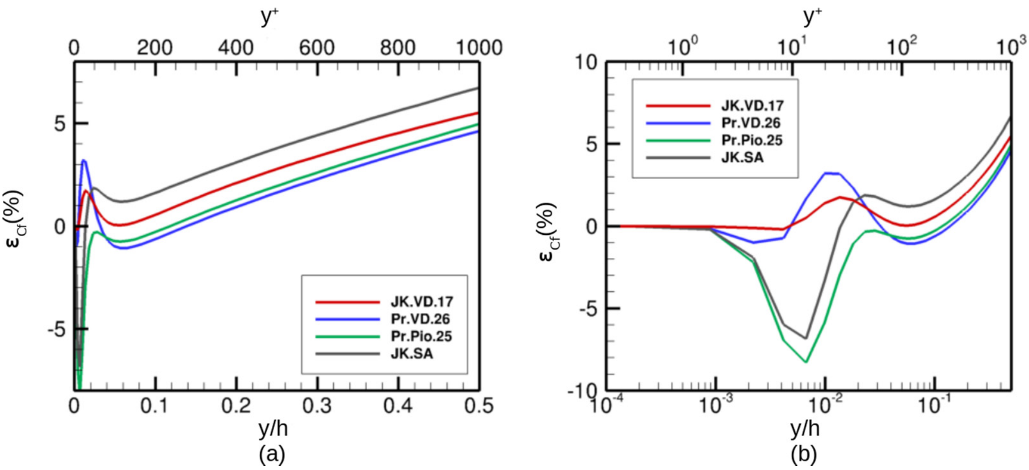

FIG. 3. Effect of different mixing-length models and damping functions on the wall-model predictions for the $\mathrm{Re}_\tau \approx 2000$ channel with (a) a linear scale and (b) a semilogarithmically scaled abscissa. The numbers in the legend indicate the value of A^+ used in the damping function.

mixing-length models for eddy viscosity and damping functions as Fig. 3 are used here. The results shown in Fig. 4 are consistent with those for the $\mathrm{Re}_\tau \approx 2000$ flow. For an exchange location between 0.05 and 0.15 (y/h for the channel and y/δ_{99} for the boundary layer), the error in skin friction is less than approximately 3% in magnitude for both the flows. Based on these results, we can be fairly confident of the accuracy of the equilibrium-wall-model predictions for incompressible flows with the chosen set of parameters (κ and A^+).

B. Compressible flows

We now perform *a priori* analysis for high-speed compressible turbulent flows. We consider a cold-wall supersonic channel flow, adiabatic supersonic boundary layer, and supersonic-through-hypersonic boundary layer over a range of thermal boundary conditions. The time-averaged velocity

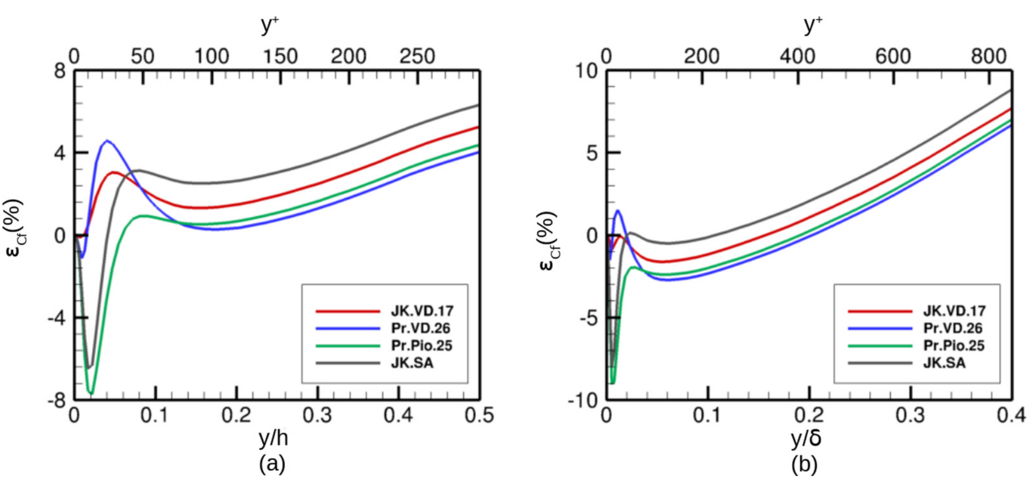

FIG. 4. Effect of different mixing-length models and damping functions on the wall-model predictions for (a) the $\mathrm{Re}_\tau = 590$ channel and (b) the $\mathrm{Re}_\tau = 2118$ turbulent boundary layer.

and temperature at different exchange locations are input to the wall model, and the error in the skin friction C_f and heat-transfer parameter B_q or wall temperature T_w are analyzed. Since we have already checked the sensitivity of the model to A^+, κ, dp/dx, and the mixing-length model for incompressible flows, we will mainly focus on the effect of the van Driest damping function scaling for the JK mixing-length model. We also report the results using the SA damping function since it is widely used for high-speed RANS. For a subset of cases, we will also examine the sensitivity to the mixing-length model and turbulent Prandtl number Pr_t.

For the results that follow, the top horizontal axis of the figure is the viscous wall scaling $y^+ = yu_\tau/\nu_w$, with $u_\tau = \sqrt{\tau_w/\rho_w}$. The standard parameters from incompressible flow are also used here, namely, $\kappa = 0.41$ and $A^+ = 17$ (for the JK model), and dp/dx is neglected for channel flows. Also, $\mathrm{Pr}_t = 0.9$ for all the results reported, even though the DNS at times predicts a somewhat different value. The viscosity-temperature relationship is chosen to match the DNS using either a power law or Sutherland's law. Our tests indicated that having a different viscosity-temperature relationship in the wall model and DNS can incur significant errors (not shown).

1. Supersonic channel flow at cold-wall conditions

We first consider the cold-wall supersonic channel flow corresponding to the DNS of Coleman *et al.* [26]. The Mach number Ma_b based on the bulk velocity and wall temperature is 1.5 and 3.0, respectively, while the Reynolds number based on the bulk density and velocity and on the wall viscosity ($\mathrm{Re} = \rho_b u_b h/\mu_w$) is 3000 and 4880, respectively. The centerline temperature T_c/T_w is 1.378 and 2.49 for Mach 1.5 and Mach 3 flows, respectively. The effect of the damping function scalings discussed in Sec. II A is shown in Fig. 5 for the JK mixing-length model. The errors in skin friction C_f and heat-transfer parameter B_q are shown for Mach 1.5 and Mach 3.0. For the Mach 1.5 case, we see that, overall, the local scaling works best followed by the mixed2 and semilocal scalings. For the Mach 3 flow, the mixed2 scaling works best for both C_f and B_q, followed by the semilocal scaling. The SA damping function also works well for these flows and behaves similarly to the semilocal scaling at larger exchange locations. The wall scaling yields the most erroneous results among all the scalings for both the flows, with semilocal giving improved predictions, consistent with previous findings of Bocquet *et al.* [11] and Yang and Lv [16]. The errors for the two flows are consistent with the values previously reported by Bocquet *et al.* [11], who used a Prandtl mixing-length model instead. Note that the Mach 3 flow has a higher B_q and a colder wall compared to Mach 1.5. Thus, for strongly cooled walls, the mixed2 scaling appears to work best. One can observe a monotonic trend in the errors as we go from the wall, mixed, semilocal, mixed2, and local scalings, with the mixed, mixed2, and semilocal scalings lying between the wall and local scalings. For cold-wall flows, $y^+_{\mathrm{wall}} > y^+_{\mathrm{SL}}$, and so the wall scaling implies lesser damping, which yields an overprediction in C_f. This is consistent with the behavior observed in the incompressible channel in Fig. 1, where an overprediction in C_f was observed for smaller values of A^+ (or larger values of y^+/A^+). We see that using an incorrect scaling for the damping function (wall scaling for cold-wall flows) can result in a significant error in the predictions (up to 100%), which was also shown by Yang and Lv [16] for a supersonic Couette flow. Also, the mixedmin (mixedmin2) scaling lies right on top of the semilocal (mixed2) scaling, which is expected for cold-wall cases. We also see that the errors are generally lower at $y/h \approx 0.05$, compared to larger values of y/h.

We also consider the cold-wall supersonic channel flow corresponding to the DNS of Modesti and Pirozzoli [29] at $\mathrm{Ma}_b = 1.5$ and $\mathrm{Re}_b = 17\,000$, with identical definitions of the two bulk parameters as before. This case has a significantly higher Reynolds number compared to the Coleman *et al.* [26] data. The errors in C_f and B_q are shown in Figs. 6(a) and 6(b), respectively. The results are qualitatively similar to those in Fig. 5 with the wall scaling overpredicting by up to 25% in both C_f and B_q and the semilocal, mixed2, and local scalings being least erroneous overall. The results also indicate that the errors are lower in magnitude at higher Reynolds numbers compared to the Mach 1.5 results in Figs. 5(a) and 5(b), consistent with the analysis of Yang and Lv [16] for supersonic Couette flow.

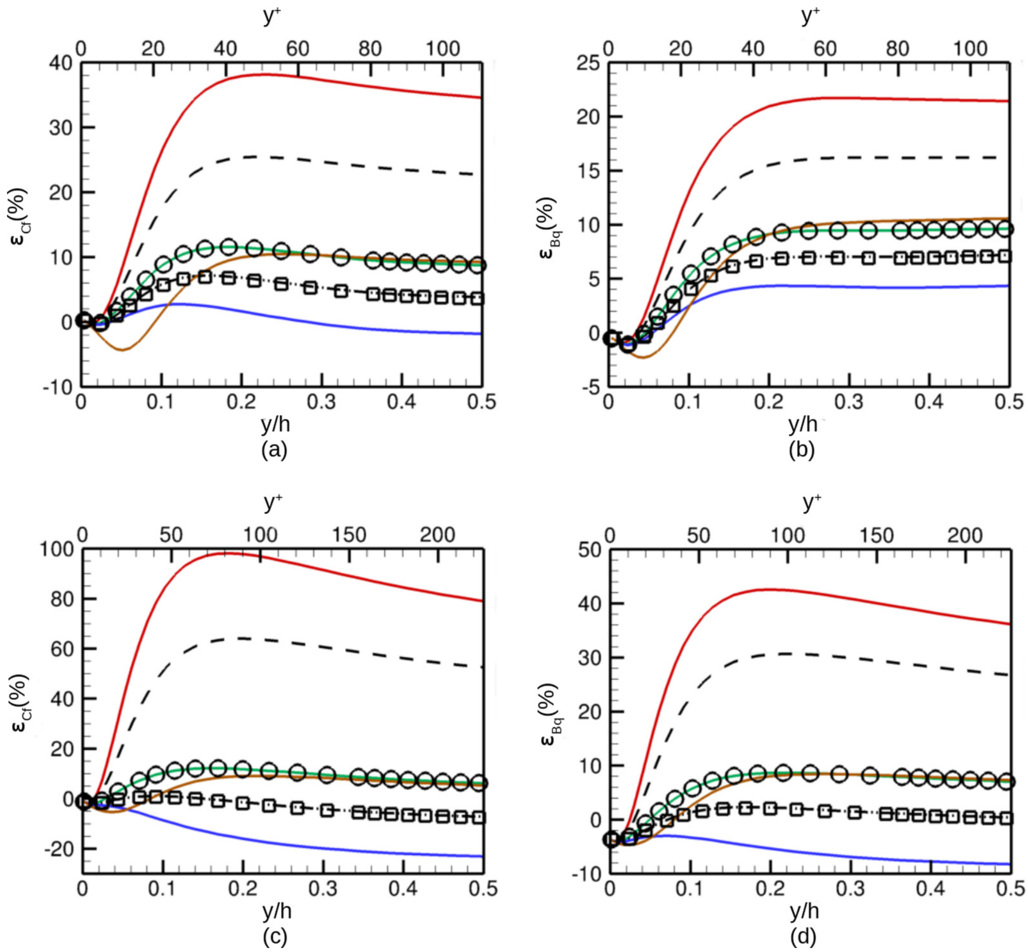

FIG. 5. Effect of damping function scalings for the wall model using the Johnson-King-based mixing-length model for (a) and (b) Mach 1.5 and (c) and (d) Mach 3 cold-wall channel flows corresponding to the DNS of Coleman *et al.* [26]. The legend is as follows: , wall; , mixed; , semilocal; .., mixed2; , local; , SA; ◯, mixedmin; and □, mixedmin2.

2. Supersonic turbulent boundary layer at adiabatic conditions

We now consider the adiabatic supersonic turbulent boundary layer corresponding to the study of Pirozzoli and Bernardini [38–41]. The freestream Mach numbers are 2 and 4 and the corresponding $\mathrm{Re}_\tau = u_\tau \delta_{99}/\nu_w$ are 1113 and 398, respectively. The errors in C_f and T_w are shown in Fig. 7. As observed for the cold-wall flows, we still see a consistent trend in the C_f prediction as we go from the wall, mixed, semilocal, mixed2, and local scalings. For adiabatic wall flows, $y^+_{\mathrm{wall}} < y^+_{\mathrm{SL}}$, and so the wall scaling implies more damping, which yields an underprediction in C_f, while the SL scaling overpredicts C_f. In general, the errors are lower for adiabatic walls when compared to cold walls. We see that the mixed scaling best predicts the C_f, to within 3% error, while the SA and semilocal damping overpredict the C_f by 5–10% at $y/\delta = 0.1$. The error of the wall and semilocal scalings for adiabatic flows appears to increase with Mach number, as observed between Mach 2 and 4 (and Mach 3 flow, which is not shown here). In terms of the wall-temperature predictions, interestingly, the different damping functions have a negligible effect, with all of them predicting nearly identical wall-temperature values. The mixedmin and mixedmin2 scalings collapse to the mixed scaling for adiabatic flow, which is most accurate for this regime, compared to the other damping function scalings.

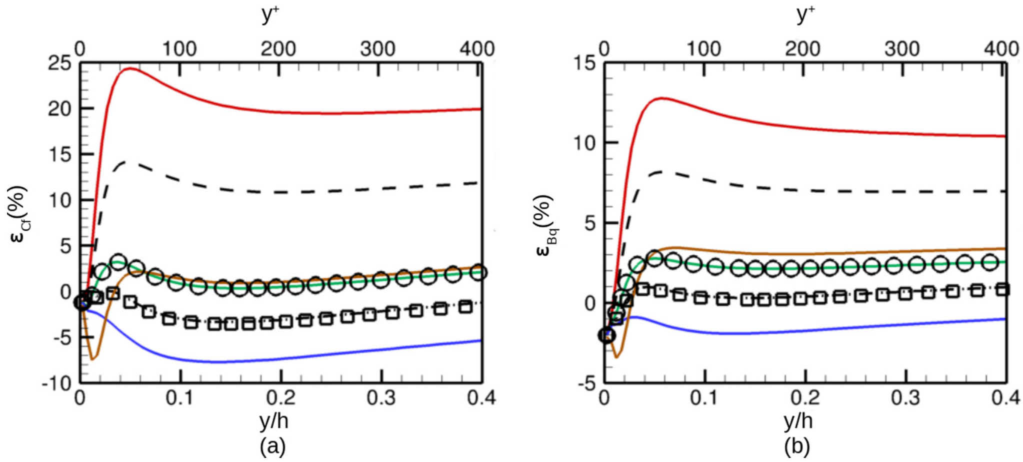

FIG. 6. Effect of damping function scalings for the wall model using the Johnson-King-based mixing-length model for Mach 1.5 cold-wall channel flow for (a) skin friction and (b) wall heat flux, corresponding to the DNS of Modesti and Pirozzoli [29]. The legend is as follows: ▬, wall; ▬ ▬, mixed; ▬, semilocal ▬ ··, mixed2; ▬, local; ▬, SA; ◯, mixedmin; and □, mixedmin2.

3. *Hypersonic turbulent boundary layer over a range of thermal conditions*

In this section, the benchmark is the recent turbulent boundary-layer database of Zhang *et al.* [28], which covers Mach numbers between 2.5 and 14, and wall-temperature conditions from cold through adiabatic conditions. Figures 8(a) and 8(b) show the predictions for a Mach 2.5 adiabatic turbulent boundary layer at $\mathrm{Re}_\tau = 510$. Generally, the findings are similar to those in Sec. III B 2 in that the mixed (and mixedmin, mixedmin2) scaling gives the best prediction overall, with under 2% error for $y/\delta_{99} < 0.1$. The wall scaling too performs well under these conditions. Again, similar to previous observations, the wall-temperature predictions by the different scalings are nearly identical for all the damping function scalings. Figures 8(c) and 8(d) show the predictions of errors in C_f and B_q for a Mach 5.86 boundary layer, with $\mathrm{Re}_\tau = 453$ and $T_w/T_{\mathrm{ad}} = 0.76$, where T_{ad} is the adiabatic recovery temperature. For this case, the wall scaling works best in terms of C_f but is more erroneous for B_q. The semilocal, mixed2, local, and SA scalings have a significant error in C_f but a lower error in B_q. Overall, the mixed scaling works best in terms of both C_f and B_q and the mixedmin and mixedmin2 scalings reduce to the mixed scaling for this flow. However, overall, the best predictions have larger errors (approximately 10%) compared to the previous (lower-Mach-number) cases.

In Fig. 9, the errors in C_f and B_q are shown for Mach 7.86 and Mach 13.68 flows, with a corresponding $\mathrm{Re}_\tau = 480$ and 646, and $T_w/T_{\mathrm{ad}} = 0.48$ and 0.18. We have so far seen that the wall scaling overpredicted C_f and B_q for cold-wall flows while it underpredicted for adiabatic conditions; thus the errors decrease from the cold to the adiabatic wall, with the opposite trend (increase in error) for the semilocal scaling. Thus, conceivably there should be a wall condition (T_w/T_{ad}) where the semilocal and wall scalings give identical results. It so happens that this occurs for the Mach 7.86 flow for $T_w/T_{\mathrm{ad}} = 0.48$, with all the scalings producing nearly identical predictions. However, at $y/\delta = 0.1$, there is significant error of approximately 20% in C_f. Also, for this condition, the mixedmin (mixedmin2) scalings do not exactly match the mixed or semilocal (mixed2) scalings, but have slightly lower error overall. This is not unexpected, as the mixedmin (mixedmin2) scalings were designed to switch between the mixed and semilocal (mixed2) scalings for adiabatic and cold walls. For the Mach 13.68 flow with a cold wall, the results are consistent with previously observed trends for the channel flow of Coleman *et al.* (Sec. III B 1). The mixed2 scaling has the least error in C_f overall and the semilocal and SA scalings have the lowest error in B_q. The mixedmin (mixedmin2) scaling matches the semilocal (mixed2) scaling for this condition.

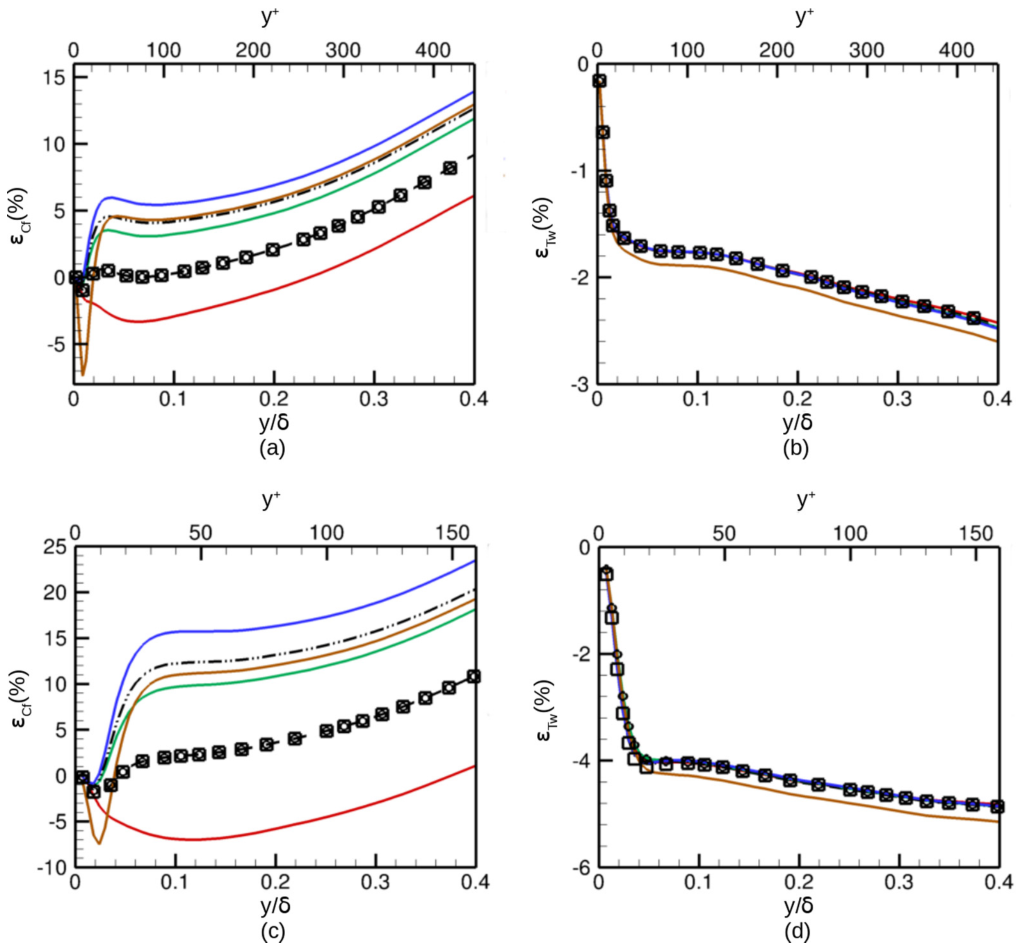

FIG. 7. Effect of damping function scalings for the wall model using the Johnson-King-based mixing-length model for (a) and (b) the Mach 2 and (c) and (d) the Mach 4 boundary layer at adiabatic conditions. The legend is as follows: ▬, wall; ▬ ▬, mixed; ▬, semilocal; ▬ ··, mixed2; ▬, local; ▬, SA; ○, mixedmin; and □, mixedmin2.

4. *Effect of mixing-length model and turbulent Prandtl number*

Figure 10 shows the errors in wall quantities, revealing the effect of the mixing-length model for the cold-wall Mach 3 channel discussed in Sec. III B 1 [Figs. 10(a) and 10(b)] and the adiabatic Mach 4 boundary layer discussed in Sec. III B 2 [Figs. 10(c) and 10(d)]. The Johnson-King-based and Prandtl mixing-length models are used. We show results corresponding to the wall and semilocal scalings for the two mixing-length models. Note that the damping function is the same for both, with $A^+ = 17$ and 26 for the JK and Pr models, respectively, based on the previously observed results for incompressible flow (Sec. III A 1). Similar to observations from incompressible results, we see that the effect of the mixing-length model is small for the different flows and scalings shown in the figure. Thus, there appears to be no compelling reason to use one model over another, provided the appropriate value for A^+ is used for the damping function.

Figure 11 shows the effect of the turbulent Prandtl number Pr_t on the wall-model errors for the Mach 3 cold-wall channel [Figs. 11(a) and 11(b)] and the adiabatic Mach 4 boundary layer [Figs. 11(c) and 11(d)]. The turbulent Prandtl number is varied between 0.6 and 2.0. For the channel

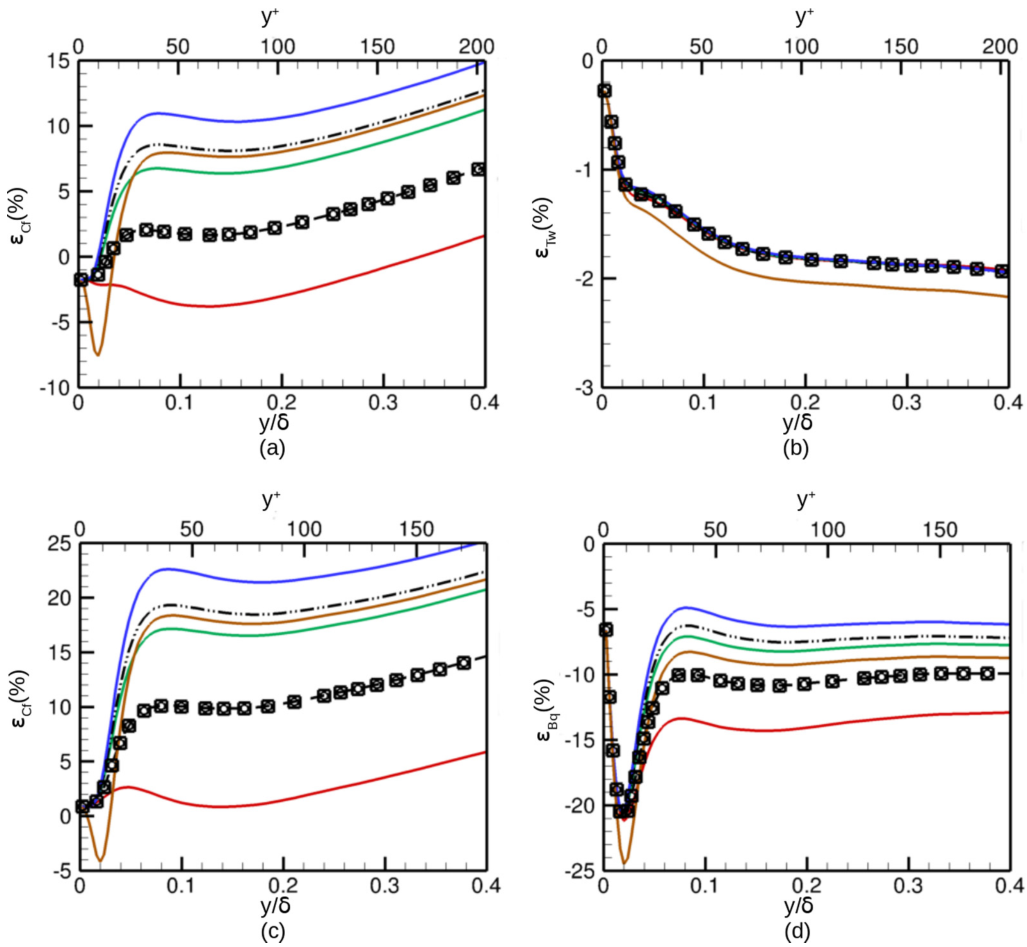

FIG. 8. Effect of damping function scalings for the wall model using the Johnson-King-based mixing-length model for (a) and (b) an adiabatic Mach 2.5 and (c) and (d) a Mach 5.86, $T_w/T_{\text{ad}} = 0.76$ boundary layer. The legend is as follows: ▬, wall; ▬ ▬, mixed; ▬, semilocal; ▬ ··, mixed2; ▬, local; ▬, SA; ◯, mixedmin; and □, mixedmin2.

flow, the influence of Pr_t on the C_f errors appear to be small but is significant for the errors in B_q with up to 15% variation. For the adiabatic boundary-layer flow, the effect of Pr_t on C_f is small until $y/\delta = 0.05$ and significant (up to 20%) beyond that. The turbulent Prandtl number also has a significant effect on the wall-temperature prediction for adiabatic flows. Although a large variation in Pr_t was assessed here, typical values of Pr_t are between 0.8 and 1.0. Thus, over this range, the effect of Pr_t may be less significant (under approximately 5%).

5. Quantitative summary of the a priori analysis of damping function scaling

We now summarize the results for the high-speed flows considered so far for the different damping function scalings in Table I. The different cases are named based on the corresponding reference. The accuracy of the results in this table is dependent on the accuracy of the corresponding DNS, which we assume to be the "truth." The turbulent Prandtl number Pr_t in the DNS also influences the results, since we have used a value of 0.9 for all the flows in this study. We estimate that the errors due to Pr_t should be small (less than 2%), based on the reported values of Pr_t in

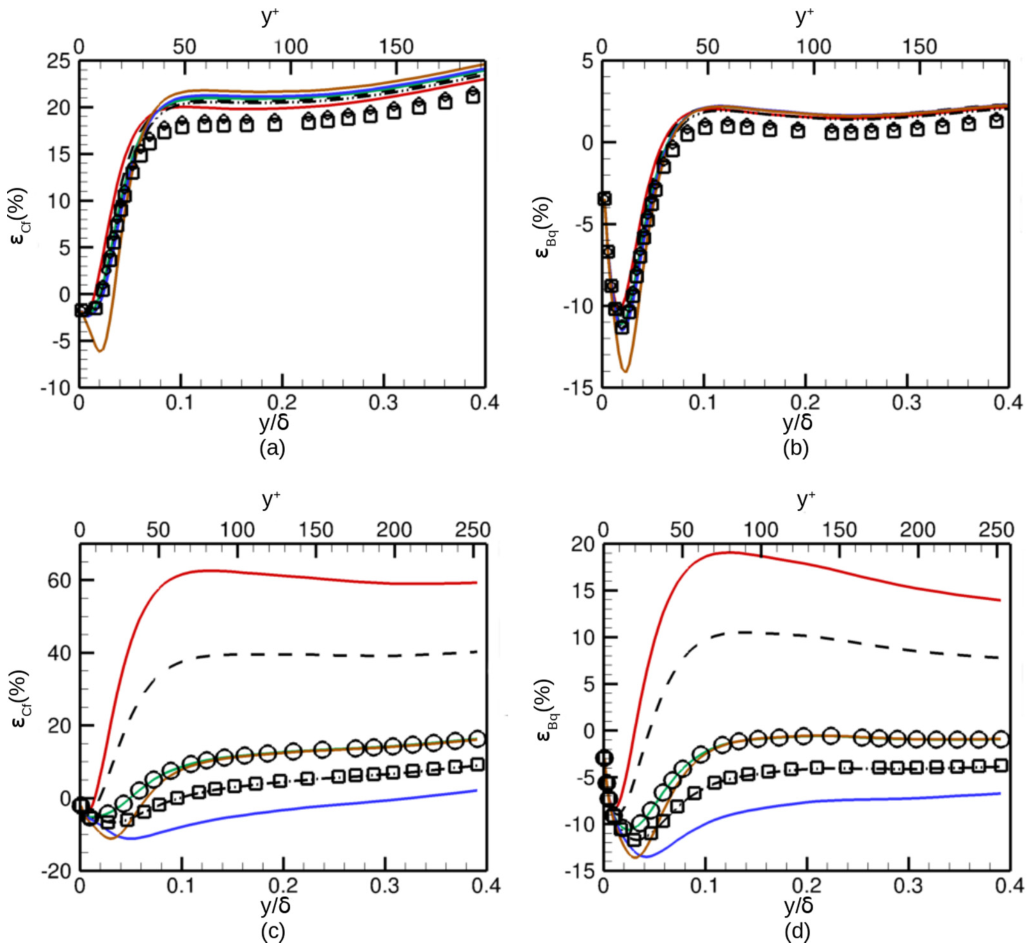

FIG. 9. Effect of damping function scalings for the wall model using the Johnson-King-based mixing-length model for (a) and (b) a Mach 7.86, $T_w/T_{\rm ad} = 0.48$ and (c) and (d) a Mach 13.68, $T_w/T_{\rm ad} = 0.18$ boundary layer. The legend is as follows: red solid line, wall; black dashed line, mixed; green solid line, semilocal, black dash-dot line, mixed2; blue solid line, local; brown solid line, SA; ○, mixedmin; and □, mixedmin2.

some of the DNS studies. The value of $T_w/T_{\rm ad}$ reported for the channel flows for comparison with the boundary-layer flows is only approximate and computed based on the centerline temperature $[1 + 0.5r(\gamma - 1)(u_b/\sqrt{\gamma R T_c})^2$ with $r = 0.89]$. Thus, the value of $T_w/T_{\rm ad}$ for internal (channel) and external (boundary-layer) flows may not be equivalent.

We report the errors ($\varepsilon_Q\%$) in C_f and B_q/T_w at y/h or y/δ of 5% and 10%, which are the typical exchange locations in WMLES studies. We report the results for the wall, semilocal, local, mixedmin, and mixedmin2 scalings for the van Driest damping function and the SA damping function. The mixed (mixed2) scaling errors are approximately the average of the wall (local) and semilocal damping scaling errors as can be observed in Figs. 5–9 and so are not reported here. The error values are colored in red, blue, and green for error magnitudes greater than 10%, 5–10%, and less than or equal to 5%, respectively. Our main focus will be on the mixedmin and mixedmin2 scalings, which reduce to the mixed scaling for hot-wall flows, and the semilocal or mixed2 scaling for cold-wall flows.

For the cold-wall channel flows corresponding to the DNS of Coleman *et al.* [26] and Modesti and Pirozzoli [29], we see that at an exchange location of 0.05, both the mixedmin and mixedmin2

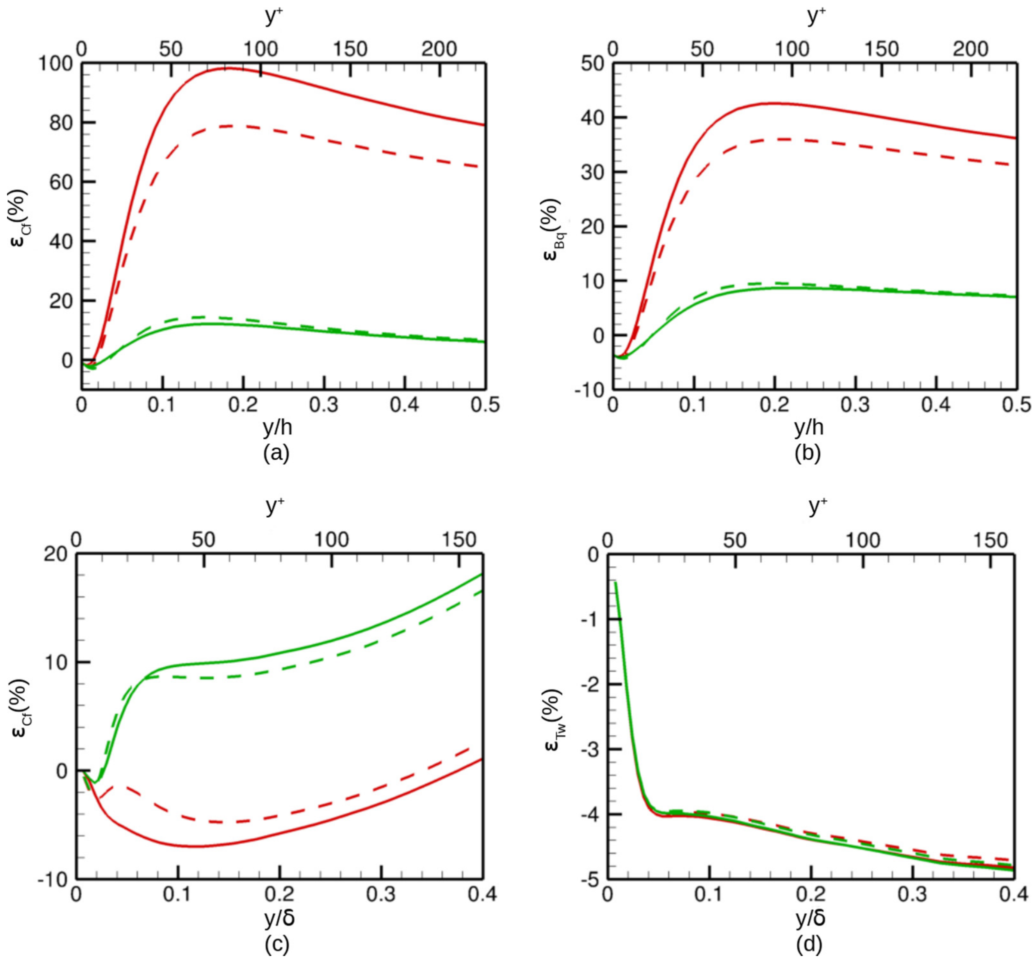

FIG. 10. Effect of the mixing-length model for (a) and (b) the cold-wall Mach 3 channel flow and (c) and (d) the adiabatic Mach 4 boundary layer. The legend is as follows: ▬, JK wall; ‒ ‒, Prandtl wall; ▬, JK semilocal; and ‒ ‒, Prandtl semilocal.

give errors under 5%, but at an exchange location of 0.1, the mixedmin2 scaling gives significantly improved predictions. The SA damping function also gives excellent results for cold-wall channel flows, with under 5% error. The wall and mixed scalings give large errors (up to 83%) for these cold-wall flows.

For the adiabatic boundary-layer flows corresponding to the DNS of Pirozzoli and Bernardini [38–41] and Zhang *et al.* [28], we see that the mixedmin and mixedmin2 scalings give the best predictions overall, with under 5% in both C_f and T_w, at both exchange locations. Note that both these scalings reduce to the mixed scaling at this condition. The semilocal and SA scalings generally have higher errors, which increase from 3–4% for Mach 2 to 8–10% for Mach 4. Presumably, based on this trend, the errors would be even higher for hypersonic flows ($\mathrm{Ma}_\infty > 5$).

For the Mach 5.86 boundary layer with $T_w/T_{\mathrm{ad}} = 0.25$ and the Mach 13.86 boundary layer with $T_w/T_{\mathrm{ad}} = 0.18$ corresponding to that of Zhang *et al.* [28], the behavior is generally consistent with the cold-wall channel flows, with the mixedmin2 scaling giving the lowest errors overall at both exchange locations. However, we see that the errors in B_q are slightly higher (5–11%) for both the mixedmin and mixedmin2 scalings, which reduce to the semilocal and mixed2 scalings, respectively.

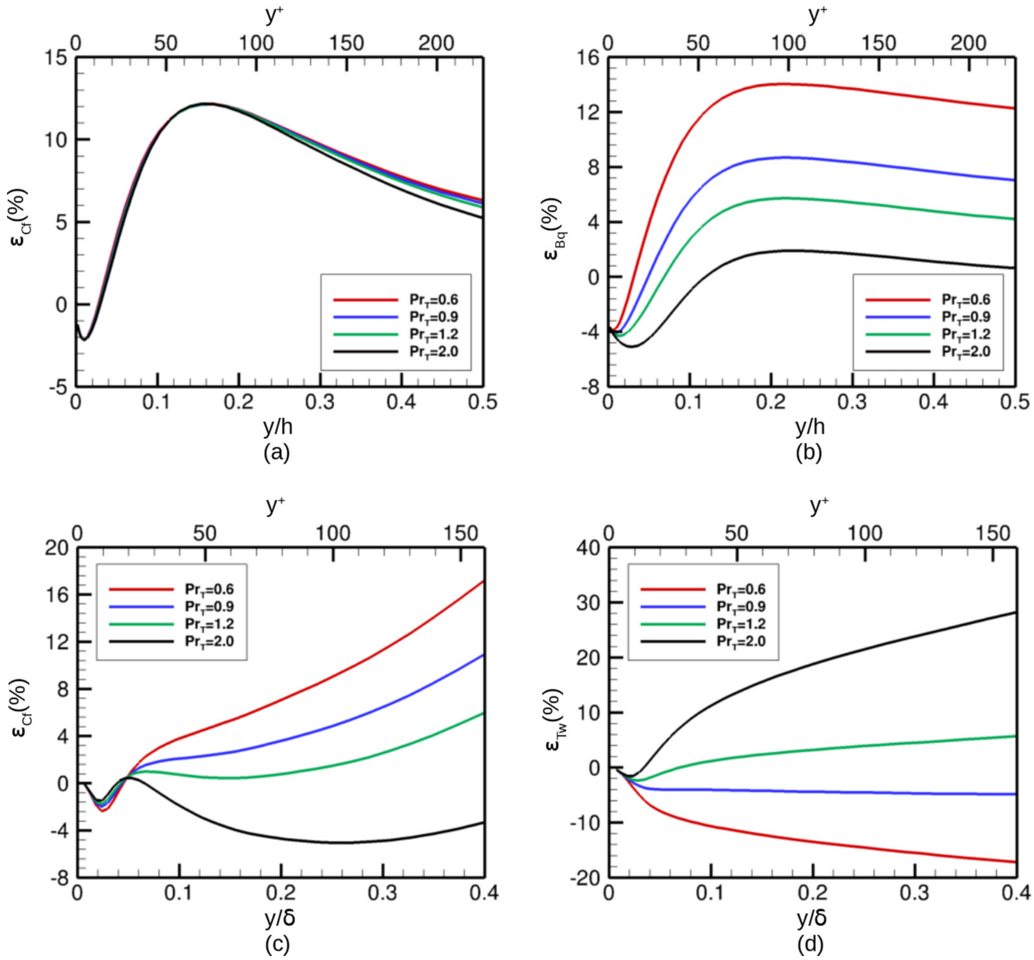

FIG. 11. Effect of the turbulent Prandtl number for the wall model using the Johnson-King-based mixing-length model and mixedmin damping function scaling for (a) and (b) the cold-wall Mach 3 channel flow and (c) and (d) the adiabatic Mach 4 boundary layer.

The performance of the SA damping function is similar to the semilocal scaling for these flows, with the wall scaling having large errors of up to 62%.

The Mach 5.86 boundary layer with $T_w/T_{\text{ad}} = 0.76$ and the Mach 7.86 boundary layer with $T_w/T_{\text{ad}} = 0.48$ corresponding to the DNS of Zhang *et al.* [28] overall have the largest errors for both the mixedmin and mixedmin2 scalings. For the Mach 5.86 case, both the mixedmin and mixedmin2 scalings reduce to the mixed scaling, with an error of up to 12%. For this case, the wall scaling has the minimum error in terms of C_f but has a large error in terms of B_q. For the Mach 7.86 flow, we see that all the scalings have similar errors, between 10% and 20% in terms of C_f, but good predictions for B_q with less than 5% error.

Overall, for all the flows, it appears that the mixedmin2 scaling provides the best predictions for both adiabatic and cold-wall flows with under 5% error in terms of both C_f and B_q or T_w. For intermediate thermal boundary conditions ($T_w/T_{\text{ad}} = 0.48, 0.76$), we see that the errors are typically larger, at approximately 10%, at an exchange location of 0.05, and up to 19% at an exchange location of 0.1. We need additional data at these intermediate conditions to attempt to improve the scalings. For the mixedmin scaling, which reduces to the semilocal scaling for cold-wall flows, the errors are

TABLE I. Errors in prediction of wall quantities (Q) at an exchange location (y/h or y/δ) of 0.05 or 0.1 are listed using the JK mixing-length model. The errors are highlighted in red, blue, and green for error magnitudes greater than 10%, 5–10%, and less than or equal to 5%, respectively.

Case	M	Re_τ	$\frac{T_w}{T_{\mathrm{ad}}}$	Q	Wall	SL	Local	SA	mixedmin	mixedmin2
Ref. [26]	1.5	222	0.46	C_f	7.9, 26.2	2.5, 8.6	0.6, 2.5	−4.3, 1.3	2.5, 8.6	1.5, 5.6
				B_q	2.6, 12.9	0.4, 5.2	−0.3, 2.5	−2.2, 2.4	0.4, 5.2	0.1, 3.8
	3.0	451	0.18	C_f	39.2, 83.2	3.9, 10.2	−3.9, −8.6	−4.8, 2.4	3.9, 10.2	0.1, 1.1
				B_q	14.2, 34.4	0.1, 5.6	−3.1, −3.3	−3.4, 2.4	0.1, 5.6	−1.6, 1.2
Ref. [29]	1.5	1011	0.46	C_f	24.4, 21.7	2.7, 0.9	−5.2, −7.4	1.9, 1.2	2.7, 0.9	−1.0, −3.0
				B_q	12.6, 12.0	2.7, 2.3	−1.2, −1.8	3.1, 3.3	2.7, 2.3	0.9, 0.4
Refs. [38–41]	2.0	1113	1.0	C_f	−3.2, −2.9	3.2, 3.3	5.7, 5.2	4.5, 4.4	0.2, 0.3	0.2, 0.3
				T_w	−1.7, −1.8	−1.7, −1.8	−1.7, −1.8	−1.9, −1.9	−1.7, −1.8	−1.7, −1.8
	3.0	502	1.0	C_f	−4.7, −5.8	5.8, 7.1	9.9, 11.7	5.7, 8.4	0.7, 1.1	0.7, 1.1
				T_w	−3.4, −3.5	−3.4, −3.5	−3.4, −3.5	−3.6, −3.7	−3.4, −3.5	−3.4, −3.5
	4.0	398	1.0	C_f	−5.3, −6.9	6.3, 9.7	11.0, 15.7	5.2, 11.0	0.6, 2.1	0.6, 2.1
				T_w	−4.0, −4.1	−4.0, −4.0	−4.0, −4.0	−4.2, −4.3	−4.0, −4.1	−4.0, −4.1
Ref. [28]	2.5	510	1.0	C_f	−2.2, −2.6	5.8, 7.2	9.2, 11.1	5.5, 8.6	1.9, 2.5	1.9, 2.5
				T_w	−3.0, −4.4	−3.0, −4.4	−3.0, −4.4	−3.0, −4.4	−3.0, −4.4	−3.0, −4.4
	5.86	450	0.25	C_f	33.3, 59.5	2.3, 9.5	−4.2, −3.1	−5.8, 6.7	2.3, 9.5	−1.0, 3.2
				B_q	6.8, 18.9	−6.2, −1.1	−9.1, −7.0	−9.7, −2.3	−6.2, −1.2	−7.6, −4.1
	5.86	453	0.76	C_f	2.7, 1.3	14.0, 17.1	18.6, 22.5	13.6, 18.3	8.5, 10.1	8.5, 10.1
				B_q	−14.0, −12.9	−8.9, −6.5	−7.0, −4.4	−10.6, −7.5	−11.3, −9.4	−11.3, −9.4
	7.86	480	0.48	C_f	16.2, 20.1	13.7, 20.7	13.0, 21.0	11.9, 21.6	12.9, 18.6	12.3, 17.7
				B_q	−1.7, 2.0	−2.9, 2.4	−3.2, 2.1	−3.9, 2.1	−3.2, 1.2	−3.6, 0.1
	13.86	646	0.18	C_f	43.2, 61.5	0.2, 8.6	−11.1, −8.0	−6.1, 7.8	0.2, 8.6	−5.0, 0.3
				B_q	9.3, 18.2	−8.4, −2.6	−13.7, −10.4	−11.1, −2.9	−8.4, −2.6	−11.0, −6.5

generally lower at an exchange location of 0.05 compared to 0.1, but for the mixedmin2 scaling which reduces to the mixed2 scaling, the errors are comparable at both exchange locations.

IV. *A POSTERIORI* WMLES

So far we have performed *a priori* analysis of wall-model prediction capabilities using the time-averaged DNS databases to identify the most suitable damping function scaling for compressible flows. We now perform *a posteriori* WMLES for a cold-wall Mach 3 channel flow and an axisymmetric Mach 2.85 boundary layer. The Johnson-King mixing-length model and the van Driest damping function with different scalings are used in the wall model. The Charles solver [45] is used in the simulations. This code solves the compressible Navier-Stokes equations on unstructured grids by using a cell-centered finite-volume methodology. The solver is second-order accurate in space for unstructured grids. An explicit third-order Runge-Kutta scheme is used for time advancement. The constant coefficient Vreman model was used to model the subgrid terms. The solver uses an essentially nonoscillatory-based reconstruction scheme with a Harten–Lax–van Leer–Contact flux for shock capturing. Further details about the numerics can be found in Ref. [46]. The solver has been applied to a wide range of problems such as shock-turbulence interaction [12], supersonic jets [47], and WMLES of turbulent separated flows [48–53].

A. Supersonic cold-wall channel flow

We perform WMLES for a supersonic cold-wall channel flow corresponding to the DNS of Coleman *et al.* [26]. The bulk Mach number ($\mathrm{Ma}_b = u_b/c_w$) and the bulk Reynolds number ($\mathrm{Re}_b = \rho_b u_b h/\mu_w$) are 3 and 4880, respectively, while the friction Reynolds number ($\mathrm{Re}_\tau = u_\tau h/\nu_w$)

TABLE II. *A priori* and *a posteriori* errors (ε_Q%) in C_f and B_q for the Mach 3 cold-wall channel flow.

Case	$y/h\|_{\mathrm{EL}}$	Wall	Mixed	mixedmin, semilocal	mixedmin2, mixed2
a priori	0.1	83.2, 34.4	51.0, 22.6	10.2, 5.6	0.7, 1.2
a posteriori	0.1	68.6, 29.1	43.4, 19.6	9.3, 5.3	0.9, 1.4

is 451. Isothermal conditions are imposed at the wall with $T_w/T_b = 0.4186$. The domain size $(L_x/h, L_y/h, L_z/h)$ used is $(16, 2, 6)$, with uniform spacings in all three directions using 16 points per channel half-width h. The corresponding grid spacings in viscous wall units are $\Delta x^+ = \Delta y^+ = \Delta z^+ = 28$. Periodic boundary conditions were imposed in the streamwise and spanwise directions, while the shear stress and heat flux from the wall model were imposed at the top and bottom walls. The exchange location at which data were input to the wall model was $y/h = 0.1$ ($y^+ \approx 45$), which corresponds to the second grid point from the wall to minimize numerical-subgrid scale errors based on the reasoning of Kawai and Larsson [10]. The simulation was driven by a source term in the x-momentum and energy equations to maintain constant bulk velocity and temperature, respectively. The source terms used were identical to the previous WMLES of Bocquet *et al.* [11] and so the details are not repeated here.

Table II shows the errors in C_f and B_q for the different damping function scalings. Note that the mixedmin (mixedmin2) scaling results are identical to semilocal (mixed2) results for this flow condition. Overall, it can be seen that the results are qualitatively similar to the *a priori* analysis results with the mixedmin2-mixed2 scalings yielding the best predictions with under 2% error at an exchange location of $y/h = 0.1$. Note that the *a priori* and *a posteriori* results are not quantitatively identical, due to other errors in the WMLES as also observed by Bocquet *et al.* [11]. However, our results are closer to the *a priori* results compared to those of Bocquet *et al.* [11], since the exchange location is further away from the wall. We also performed additional simulations for the wall and semilocal scalings using a finer grid, with twice the resolution in each direction, and the results did not vary significantly.

Figure 12 shows the variation of the time-averaged velocity, temperature, and total turbulent shear stress (modeled plus resolved) with the wall-normal coordinate y, and velocity in inner units, for the different damping function scalings used, is compared with the DNS results. Since we are imposing the bulk velocity and temperature in the simulation, the velocity and temperature when scaled with the bulk quantities are nearly identical for all the damping function scalings and match well with DNS. Errors up to 5% in the velocity and temperature are expected based on the corresponding errors in the wall quantities from the *a priori* analysis. The turbulent shear stress $\overline{u'v'}$ is best predicted by the mixedmin2-mixed2 scalings. Likewise, when plotted in inner units ($u^+ = u/u_\tau$), the semilocal and mixed2 scalings agree well with DNS, while the mixed and wall scalings show a large error due to the erroneous C_f predicted. Overall, the mixedmin2 scaling yields the best predictions.

B. Axisymmetric supersonic boundary layer at adiabatic conditions

We next simulate an axisymmetric supersonic boundary layer interacting with a compression corner corresponding to the experimental conditions of Dunagan *et al.* [54]. The freestream Mach number Ma_∞ is 2.85 and the freestream unit Reynolds number ($\mathrm{Re} = \rho_\infty u_\infty/\mu_\infty$) is $18 \times 10^6\ \mathrm{m}^{-1}$. This corresponds to $\mathrm{Re}_\theta = \rho_\infty u_\infty \theta/\mu_\infty \approx 12\,000$ at a station 4.5 cm upstream of the compression corner. We simulate a portion of the experimental domain with an azimuthal extent of 30°. The inflow of the computational domain is 30 cm upstream of the compression corner where the boundary-layer thickness $\delta_{\mathrm{in}} \approx 0.8$ cm. The grid contained about 22 points per δ_{in} in the streamwise and wall-normal directions and 50 points per δ_{in} in the spanwise direction, with a total grid count of 2×10^6. The corresponding grid spacings in viscous wall units are $\Delta x^+ = \Delta y_w^+ = 50$ and

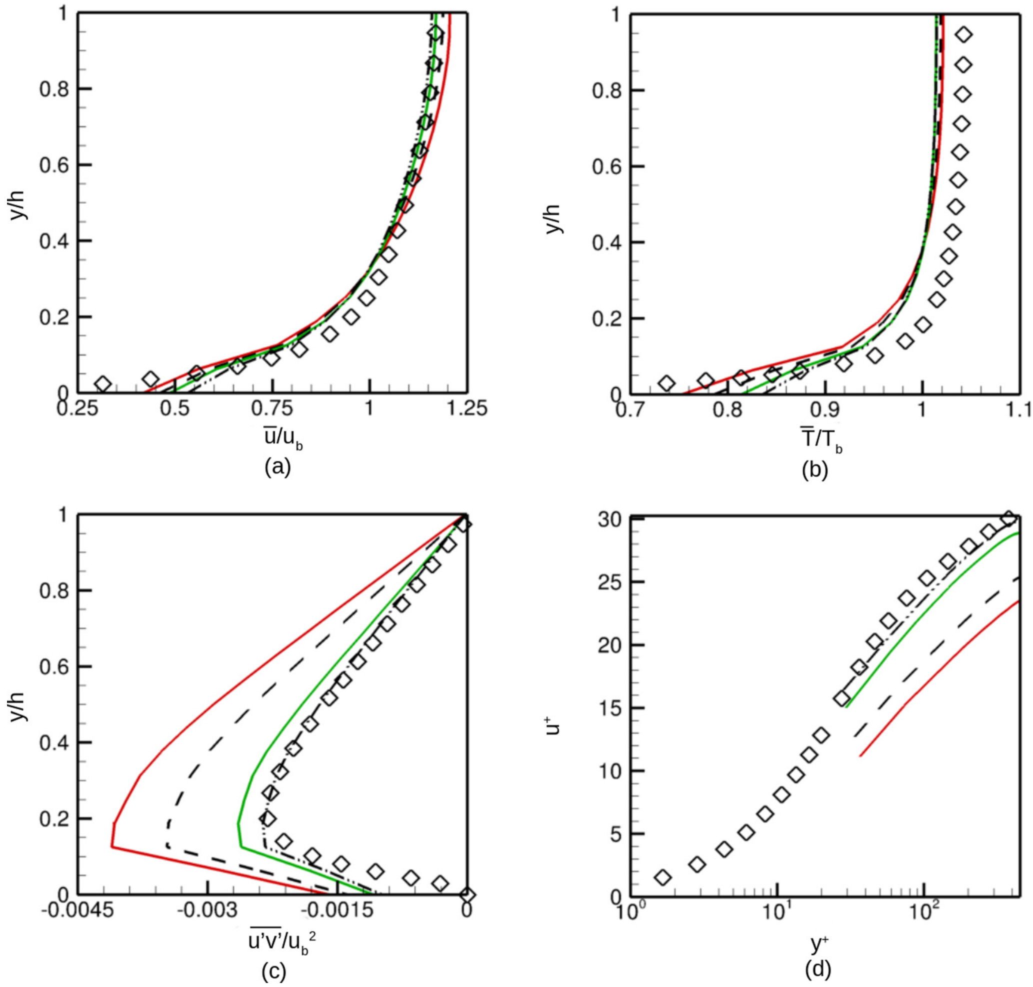

FIG. 12. Variation of (a) time-averaged velocity (u/u_b), (b) temperature (T/T_b), (c) turbulent shear stress ($\overline{u'v'}/u_b^2$), and (d) velocity in inner units (u^+) for different damping function scalings for the Mach 3 channel flow. The legend is as follows: ▬, wall; ▬ ▬, mixed; ▬, semilocal and mixedmin; ▬··, mixed2 and mixedmin2; and $\diamond$, DNS of Coleman *et al.* [26].

$\Delta z^+ = 20$ at 4.5 cm upstream of the compression corner. The mean velocity, temperature and turbulent stresses at the inflow were specified using SA RANS, and a synthetic inflow-turbulence generator based on the method of Shur *et al.* [55] was used to generate fluctuations at the inflow plane. More details about the computational setup can be found in Ref. [53]. The WMLES results were relatively insensitive to the grid resolution in the attached portion of the domain and to an increase in the azimuthal domain size to 90° [53]. Hence, we will only discuss the results for the coarse grid here.

The *a priori* and *a posteriori* errors at 25 cm from the inflow plane ($x/\delta_{\text{in}} \approx 31$) are reported in Table III for the wall, mixed, and semilocal scalings and are consistent with previous adiabatic results in Table I. The *a priori* analysis was performed using the SA RANS mean flow data. Note that the mixed2 scaling result is worse than semilocal and so is not shown, and the mixed and mixedmin scalings are identical to the mixedmin2 scaling under this condition. The mixedmin2 scaling gives the best results overall, although the errors in the wall and semilocal scalings are small at this Ma_∞

TABLE III. *A priori* and *a posteriori* errors in C_f and T_w for Mach 2.85 adiabatic axisymmetric boundary-layer flow.

Case	$y/\delta\|_{\mathrm{EL}}$	Wall	Semilocal	mixedmin2, mixedmin, mixed
a priori	0.08	−5.6, 0.03	3.6, 0.03	−0.74, 0.03
a posteriori	0.08	−2.2, −0.18	4.3, 0.22	1.9, −0.17

and Re_θ. It is interesting that although the mean flow specified was from SA RANS, the *a priori* analysis did not show any bias towards the semilocal scaling which was closest to the SA damping function, as observed in the preceding section. The variation of C_f upstream of the compression corner is shown in Fig. 13. The inflow plane is located 30 cm upstream of the compression corner and the inflow boundary-layer thickness (δ_{99}) is 0.8 cm. Overall, we see that the mixedmin2 scaling agrees best with the SA RANS result, although the errors in the other scalings are small. A transient region associated with the inflow turbulence generation can be observed in Fig. 13 until $x/\delta_{\mathrm{in}} \approx 20$, indicated by a drop in C_f.

Figure 14 shows the wall-normal variation of $\overline{u}/u_\infty$, $\overline{u'v'}/u_\infty^2$, and velocity in inner units (u^+) at $x = -4.5$ cm and $\overline{\rho}/\rho_\infty$ at $x = -5.03$ cm. These were the locations at which experimental data were available. Similar to the results for the channel flow, we see that when the quantities are scaled with the outer units (freestream values), the velocity and density profiles are nearly identical for all the scalings. Some differences show up in the turbulent shear stress, which typically scales in inner units (u_τ). Also, in the $\overline{u'v'}$ profiles it can be seen that the results are erroneous very near the wall, due to the coarse wall-normal resolution ($\Delta y_w^+ = 50$) used. The velocity variation in the inner units shows that the mixedmin2 scaling is closest to the SA RANS. Overall, the agreement with experiment is good, but the results are closer to the SA RANS results since this was used to provide the mean flow for the inflow turbulence generator.

V. CONCLUSION

We analyzed the predictive ability of an equilibrium wall model for high-speed wall-bounded turbulent flows using *a priori* and *a posteriori* analyses. For the *a priori* analysis, the time-averaged

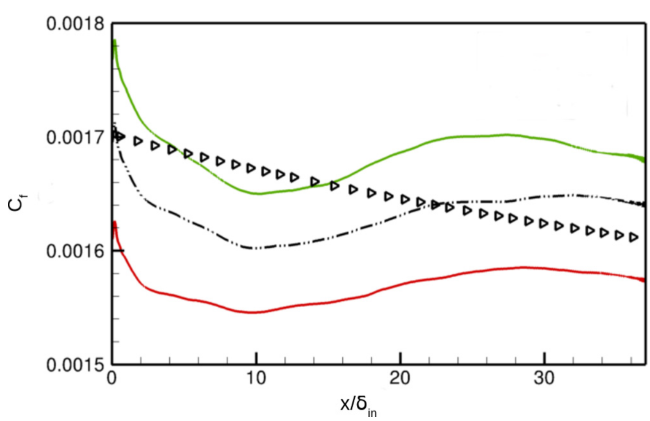

FIG. 13. Variation of C_f in the zero-pressure-gradient region upstream of the compression corner for the different damping function scalings. The legend is as follows: red line, wall; black dash-dot line, mixed, mixedmin, and mixedmin2; green line, semilocal; and ▷, SA RANS.

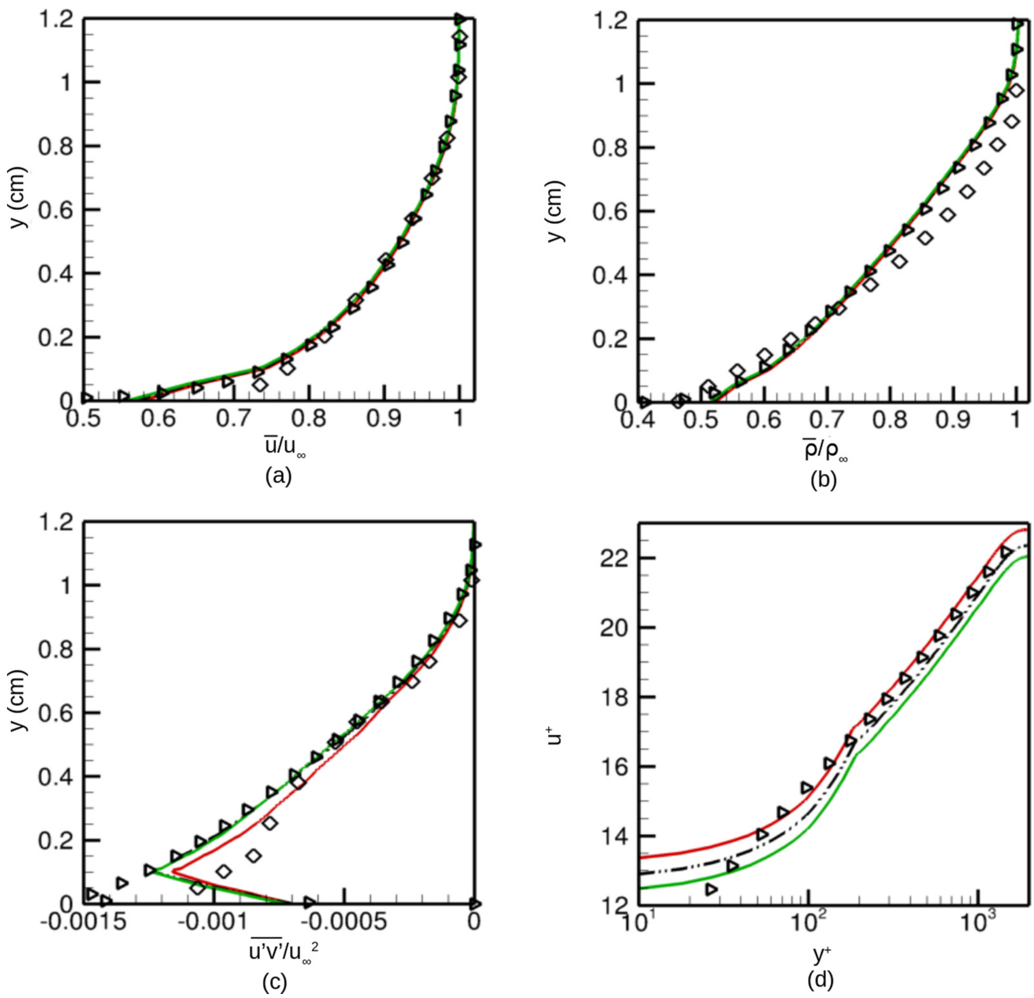

FIG. 14. Variation of time-averaged (a) velocity (u/u_∞), (b) density (ρ/ρ_∞), (c) turbulent shear stress ($\overline{u'v'}/u_\infty^2$), and (d) velocity in inner units (u^+) for different damping function scalings for the Mach 2.85 boundary-layer flow at $x/\delta_{\rm in} \approx 31$. The legend is as follows: red line, wall; black dash-dot-dot line, mixed, mixedmin, and mixedmin2; green line, semilocal; ▷, SA RANS; and ◇, experiments of Dunagan *et al.* [54].

flow parameters from various DNS databases were used as input to the wall model to assess the accuracy of the outputs with respect to the values obtained from DNS. Two mixing-length models and multiple damping function scalings for the van Driest damping function were studied. For the *a priori* analysis, we first looked at incompressible flows to assess the sensitivity of the wall model to various parameters, such as the mixing-length model used, von Kármán constant κ, empirical constant in the damping function A^+, and inclusion of the pressure gradient for channel flows. The results confirmed that the values used in most studies, with $\kappa = 0.41$ and $A^+ = 26$ for the Prandtl mixing-length model and $A^+ = 17$ for the Johnson-King-based zero-equation model, were optimal. The predictions of both the mixing-length models were of comparable accuracy. We also looked at multiple damping functions, which include the van Driest, a Spalart-Allmaras-based, and a modified van Driest–type function; again the performance of all were of comparable accuracy. The effect of including the pressure-gradient term for channel flows was small when the exchange location was less than 10% of the channel half-width. Overall, good predictive accuracy was observed for incompressible flows with under 5% error (and even lesser depending on the exchange location) in predicting C_f.

We then assessed the predictive ability for high-speed compressible flows for thermal boundary conditions ranging from cold through adiabatic walls. The optimal values of κ and A^+ for incompressible flows were used to be consistent. Multiple damping function scalings for the van Driest damping function were studied which include the wall, mixed, semilocal, mixed2, local, mixedmin, and mixedmin2 scalings. All these damping function scalings conform to the basic requirement of the damping function ($D \to 0$ as $y \to 0$, and $D \approx 1$ for $y^+ \gtrsim 30$) and reduce to the incompressible scaling at low speeds. Note that one could instead fix the damping function scaling and vary the A^+ depending on the flow conditions to obtain accurate results. However, this would make the values specific to flow conditions. We instead prefer to use the incompressible values of the empirical constants and come up with a general wall-normal scaling for the damping function that would yield the best results irrespective of the flow conditions. The wall and semilocal scalings have been used in previous WMLES studies, with the semilocal scaling yielding better predictions for cold-wall flows. We proposed damping scalings such as mixed and mixed2, whose predictions lie between the semilocal and either wall or local scalings, respectively. Depending on the thermal boundary condition, y^+_{wall} would be higher (cold walls) or lower (hot walls) than y^+_{local} and y^+_{SL}. A higher value of y^+_{wall} implies lower damping and correspondingly an overprediction in C_f. Thus, the wall scaling overpredicted C_f for cold-wall flows and underpredicted C_f for adiabatic flows, with the opposite trend for the semilocal or local scalings. The mixed and mixed2 scalings were motivated by empirical observations to reduce errors in the prediction of wall quantities. It was observed that the mixed scaling gave the best predictions for adiabatic conditions in terms of both C_f and T_w, with under 5% error in both. Overall, the mixed2 scaling gave the best predictions in terms of both C_f and B_q for cold-wall flows, with under 5% error in both. The semilocal scalings also gave acceptable predictions for cold-wall flows, although the errors were higher at farther exchange locations. The mixedmin (mixedmin2) scalings were designed to automatically switch to the mixed scaling for hot walls and semilocal (mixed2) scalings for cold walls. For the boundary-layer flows with intermediate-thermal-wall conditions, with $T_w/T_{\mathrm{ad}} = 0.48$ and 0.76, the wall-model errors were generally higher (10–18%) when compared to cold-wall ($T_w/T_{\mathrm{ad}} < 0.3$) and adiabatic cases. Note that multiple DNS databases were available and used for the analysis at cold-wall and adiabatic conditions, thus providing a higher confidence in the inferences. However, for the intermediate-wall-temperature boundary-layer cases, only a single DNS database was available and so these need to be verified with other studies. We also looked at sensitivity to the mixing-length model and found that similar to incompressible flows, both mixing-length models used were of comparable accuracy. The sensitivity to the turbulent Prandtl number Pr_t indicated that it is around 5% in terms of C_f and B_q or T_w for values ranging between 0.8 and 1.0. Overall, a value of 0.9 seemed to be a reasonable value to use.

A posteriori WMLESs were performed for a Mach 3 channel flow with a cold wall and a Mach 2.85 axisymmetric boundary layer at adiabatic conditions, and the results obtained using different scalings for the van Driest damping function were qualitatively consistent with the *a priori* analysis performed using DNS databases. The mixedmin2 scaling gave the best predictions for both flows in terms of wall quantities (C_f, B_q, or T_w) and in terms of the wall-normal variation of the time-averaged velocity (in terms of both inner and outer scalings), temperature (or density), and stresses. Some small quantitative differences were observed between the *a priori* and *a posteriori* results owing to *a posteriori* errors such as discretization and subgrid-scale modeling errors, among others.

Overall, based on the analysis over a range of thermal conditions and Mach numbers, we recommend the van Driest damping function with the mixedmin2 scaling for compressible flows and an exchange location close to 10% of the boundary-layer thickness (δ_{99}) or channel half-width h. The mixedmin2 scaling for the van Driest damping function gave consistently lower errors compared to other scalings, typically less than 5% in C_f and B_q or T_w for most of the flows considered in this study. While our focus in this study was on WMLES, the mixedmin2 scaling should be equally applicable to RANS models which use a van Driest–type damping function such as the

Baldwin-Lomax model [56]. The mixedmin2 scaling was arrived at based on empirical observations in this study and therefore is by no means a perfect scaling. However, we hope that the trends observed in this study for different scalings would lead to a more theoretically rigorous and accurate scaling in the future.

ACKNOWLEDGMENTS

This research was sponsored by the NASA Transformational Tools and Technologies Project of the Transformative Aeronautics Concepts Program under the Aeronautics Research Mission Directorate. The work of P.S.I. was sponsored by NASA under Cooperative Agreement No. NNL09AA00A. We thank Cascade Technologies for providing the Charles solver and consultation in use of the code, and Gary Coleman, Ponnampalam Balakumar, Balaji Venkatachari, Chris Rumsey, and Steven Bauer for comments on the manuscript.

---

[1] P. Spalart, W.-H. Jou, M. Strelets, and S. Allmaras, Comments on the feasibility of LES for wings, and on a hybrid RANS/LES approach, in *Proceedings of 1st AFOSR International Conference on Advances in DND/LES: Direct numerical simulation and large eddy simulation, Ruston, LA* (Greyden Press, 1997) pp. 137–148.

[2] W. Cabot and P. Moin, Approximate wall boundary conditions in the large-eddy simulation of high Reynolds number flow, Flow Turbul. Combust. **63**, 269 (2000).

[3] U. Piomelli and E. Balaras, Wall-layer models for large-eddy simulations, Annu. Rev. Fluid Mech. **34**, 349 (2002).

[4] J. Larsson, S. Kawai, J. Bodart, and I. Bermejo-Moreno, Large eddy simulation with modeled wall-stress: Recent progress and future directions, Mech. Eng. Rev. **3**, 15 (2016).

[5] S. T. Bose and G. I. Park, Wall-modeled large-eddy simulation for complex turbulent flows, Annu. Rev. Fluid Mech. **50**, 535 (2018).

[6] P. R. Spalart, Detached-eddy simulation, Annu. Rev. Fluid Mech. **41**, 181 (2009).

[7] S. Deck, Zonal-detached-eddy simulation of the flow around a high-lift configuration, AIAA J. **43**, 2372 (2005).

[8] P. R. Spalart, S. Deck, M. Shur, K. Squires, M. K. Strelets, and A. Travin, A new version of detached-eddy simulation, resistant to ambiguous grid densities, Theor. Comput. Fluid Dyn. **20**, 181 (2006).

[9] M. L. Shur, P. R. Spalart, M. K. Strelets, and A. K. Travin, A hybrid RANS-LES approach with delayed-DES and wall-modelled LES capabilities, Int. J. Heat Fluid Flow **29**, 1638 (2008).

[10] S. Kawai and J. Larsson, Wall-modeling in large eddy simulation: Length scales, grid resolution, and accuracy, Phys. Fluids **24**, 015105 (2012).

[11] S. Bocquet, P. Sagaut, and J. Jouhaud, A compressible wall model for large-eddy simulation with application to prediction of aerothermal quantities, Phys. Fluids **24**, 065103 (2012).

[12] I. Bermejo-Moreno, L. Campo, J. Larsson, J. Bodart, D. Helmer, and J. K. Eaton, Confinement effects in shock wave/turbulent boundary layer interactions through wall-modelled large-eddy simulations, J. Fluid Mech. **758**, 5 (2014).

[13] X. I. A. Yang, J. Urzay, S. Bose, and P. Moin, Aerodynamic heating in wall-modeled large-eddy simulation of high-speed flows, AIAA J. **56**, 731 (2017).

[14] E. V. Driest, On turbulent flow near a wall, J. Aeronaut. Sci. **23**, 1007 (1956).

[15] B. Aupoix and S. Viala, Compressible turbulent boundary layer modelling, Transit. Turbul. Compress. Flows **224**, 139 (1995).

[16] X. I. Yang and Y. Lv, A semi-locally scaled eddy viscosity formulation for LES wall models and flows at high speeds, Theor. Comput. Fluid Dyn. **32**, 617 (2018).

[17] D. A. Johnson and L. King, A mathematically simple turbulence closure model for attached and separated turbulent boundary layers, AIAA J. **23**, 1684 (1985).

[18] W. Cabot, Large-eddy simulations with wall models, Technical Report No. NASA-CR-200667, Stanford University Center for Turbulence Research Annual Research Briefs, 1995.
[19] L. Prandtl, Bericht uber untersuchungen zur ausgebildeten turbulenz, Z. Angew. Math. Mech. **5**, 136 (1925).
[20] E. R. van Driest, Turbulent boundary layer in compressible fluids, J. Aeronaut. Sci. **18**, 145 (1951).
[21] P. Bradshaw, Turbulence: The chief outstanding difficulty of our subject, Exp. Fluids **16**, 203 (1994).
[22] P. Huang, P. Bradshaw, and T. Coakely, Turbulence models for compressible boundary layers, AIAA J. **32**, 735 (1994).
[23] P. R. Spalart and S. R. Allmaras, A one-equation turbulence model for aerodynamic flows, Recherche Aerospatiale **1**, 5 (1994).
[24] G. Mellor and H. Herring, Two methods of calculating turbulent boundary layer behavior based on numerical solutions of the equations of motion, in *Proceedings of the AFOSR-IFP-Stanford Conference on Computation of Turbulent Boundary Layers, Stanford, 1968* (Stanford University, Stanford, 1968), pp. 18–25.
[25] U. Piomelli, J. Ferziger, P. Moin, and J. Kim, New approximate boundary conditions for large eddy simulations of wall-bounded flows, Phys. Fluids A **1**, 1061 (1989).
[26] G. N. Coleman, J. Kim, and R. Moser, A numerical study of turbulent supersonic isothermal-wall channel flow, J. Fluid Mech. **305**, 159 (1995).
[27] A. Trettel and J. Larsson, Mean velocity scaling for compressible wall turbulence with heat transfer, Phys. Fluids **28**, 026102 (2016).
[28] C. Zhang, L. Duan, and M. M. Choudhari, Direct numerical simulation database for supersonic and hypersonic turbulent boundary layers, AIAA J. **56**, 4297 (2018).
[29] D. Modesti and S. Pirozzoli, Reynolds and Mach number effects in compressible turbulent channel flow, Int. J. Heat Fluid Flow **59**, 33 (2016).
[30] R. D. Moser, J. Kim, and N. N. Mansour, Direct numerical simulation of turbulent channel flow up to $\mathrm{Re}_\tau = 590$, Phys. Fluids **11**, 943 (1999).
[31] http://turbulence.ices.utexas.edu/data/MKM/chan590/ (last accessed 10 January 2019).
[32] M. Lee and R. D. Moser, Direct numerical simulation of turbulent channel flow up to $\mathrm{Re}_\tau \approx 5200$, J. Fluid Mech. **774**, 395 (2015).
[33] http://turbulence.ices.utexas.edu/channel2015/content/Data_2015_2000.html (last accessed 10 January 2019).
[34] G. Eitel-Amor, R. Örlü, and P. Schlatter, Simulation and validation of a spatially evolving turbulent boundary layer up to $\mathrm{Re}_\theta = 8300$, Int. J. Heat Fluid Flow **47**, 57 (2014).
[35] ftp://ftp.mech.kth.se/pub/pschlatt/DATA/TBL/SIM/RE8000/ (last accessed 10 January 2019).
[36] https://turbmodels.larc.nasa.gov/Other_DNS_Data/supersonic-channel.html (last accessed 10 January 2019).
[37] http://newton.dima.uniroma1.it/supchan/ (last accessed 10 January 2019).
[38] S. Pirozzoli and M. Bernardini, Turbulence in supersonic boundary layers at moderate Reynolds number, J. Fluid Mech. **688**, 120 (2011).
[39] S. Pirozzoli and M. Bernardini, Probing high-Reynolds-number effects in numerical boundary layers, Phys. Fluids **25**, 021704 (2013).
[40] M. Bernardini and S. Pirozzoli, Wall pressure fluctuations beneath supersonic turbulent boundary layers, Phys. Fluids **23**, 085102 (2011).
[41] M. Bernardini and S. Pirozzoli, Inner/outer layer interactions in turbulent boundary layers: A refined measure for the large-scale amplitude modulation mechanism, Phys. Fluids **23**, 061701 (2011).
[42] http://reynolds.dma.uniroma1.it/dnsm2/stat/ (last accessed 10 January 2019).
[43] https://turbmodels.larc.nasa.gov/Other_DNS_Data/supersonic_hypersonic_flatplate.html (last accessed 10 January 2019).
[44] A. Lozano-Durán and J. Jiménez, Effect of the computational domain on direct simulations of turbulent channels up to $\mathrm{Re}_\tau = 4200$, Phys. Fluids **26**, 011702 (2014).
[45] Cascade Technologies, http://www.cascadetechnologies.com (last accessed 10 January 2018).

[46] Y. Khalighi, F. Ham, J. Nichols, S. Lele, and P. Moin, Unstructured Large Eddy Simulation for Prediction of Noise Issued from Turbulent Jets in Various Configurations, in *Proceedings of the 17th AIAA/CEAS Aeroacoustics Conference (32nd AIAA Aeroacoustics Conference), Portland, 2011* (AIAA, Reston, 2011), paper 2011-2886.

[47] G. A. Brès, F. E. Ham, J. W. Nichols, and S. K. Lele, Unstructured large-eddy simulations of supersonic jets, AIAA J. **55**, 1164 (2017).

[48] P. Balakumar, G. Park, and B. Pierce, DNS, LES, and wall-modeled LES of separating flow over periodic hills, in *Proceedings of the 2014 Summer Program on Studying Turbulence Using Numerical Simulation Databases—XV* (Stanford University, Stanford, 2014).

[49] P. S. Iyer and M. R. Malik, Wall-modeled large eddy simulation of flow over a wall-mounted hump, in *Proceedings of the 46th AIAA Fluid Dynamics Conference, Washington, DC, 2016* (AIAA, Reston, 2016), paper 2016-3186.

[50] P. S. Iyer, G. I. Park, and M. R. Malik, A comparative study of wall models for LES of turbulent separated flow, in *Proceedings of the 2016 Summer Program on Studying Turbulence Using Numerical Simulation Databases—XVI* (Stanford University, Stanford, 2016).

[51] G. I. Park, Wall-modeled large-eddy simulation of a high Reynolds number separating and reattaching flow, AIAA J. **55**, 3709 (2017).

[52] P. S. Iyer, G. I. Park, and M. R. Malik, Wall-modeled large eddy simulation of transonic flow over an axisymmetric bump with shock-induced separation, in *Proceedings of the 23rd AIAA Computational Fluid Dynamics Conference, Denver, 2017* (AIAA, Reston, 2017), paper 2017-3953.

[53] P. S. Iyer and M. R. Malik, Large-eddy simulation of axisymmetric compression corner flow, in *Proceedings of the 2018 Fluid Dynamics Conference, Atlanta, 2018* (AIAA, Reston, 2018), paper 2018-4031.

[54] S. E. Dunagan, J. L. Brown, and J. B. Miles, Interferometric data for a shock-wave/boundary-layer interaction, NASA Report No. NASA-TM-88227, NASA Ames Research Center, CA, United States, 1986.

[55] M. L. Shur, P. R. Spalart, M. K. Strelets, and A. K. Travin, Synthetic turbulence generators for rans-les interfaces in zonal simulations of aerodynamic and aeroacoustic problems, Flow Turbul. Combust. **93**, 63 (2014).

[56] B. Baldwin and H. Lomax, Thin-layer approximation and algebraic model for separated turbulentflows, *Proceedings of the 16th Aerospace Sciences Meeting, Huntsville, 1978* (AIAA, Reston, 1978), paper 1978-257.